

UNIVERSITY OF OKLAHOMA

GRADUATE COLLEGE

GALLING OF STAINLESS STEELS IN LOW STATIC CONTACT AND HIGH
CYCLE APPLICATIONS

A THESIS

SUBMITTED TO THE GRADUATE FACULTY

in partial fulfillment of the requirements for the

Degree of

MASTER OF SCIENCE

By

PAUL HATCH
Norman, Oklahoma
2016

GALLING OF STAINLESS STEELS IN LOW STATIC CONTACT AND HIGH
CYCLE APPLICATIONS

A THESIS APPROVED FOR THE
SCHOOL OF INDUSTRIAL AND SYSTEMS ENGINEERING

BY

Dr. Shivakumar Raman, Chair

Dr. Theodore B. Trafalis

Dr. Randa L. Shehab

© Copyright by PAUL HATCH 2016
All Rights Reserved.

This work is dedicated to my wife who has patiently awaited its completion.

Acknowledgements

This project would not have been possible without the assistance and support from Mercer Valve Company and its employees. Mercer Valve Company provided the testing laboratory and the pressure relief valve and its components used in this work. As the employer of the author, Mercer Valve Company provided opportunity and resources which significantly enable this study.

Table of Contents

Acknowledgements	iv
List of Tables	vii
List of Figures.....	viii
Abstract.....	xi
Chapter 1: Purpose of Study.....	1
Chapter 2: Theory and Literature Review	6
Friction	6
Wear Mechanisms	11
Metallurgy	21
Flash Temperature Concept.....	26
Pressure Relief Valves.....	34
Chapter 3: Methodology.....	47
CFD Simulation.....	47
Physical Testing.....	51
Chapter 4: Findings	57
CFD Simulation Results	57
Physical Testing.....	60
Conventional Model	68
Chapter 5: Discussion.....	71
Chapter 6: Final Remarks.....	86
References	89
Appendix A: PRV Specification Sheet and Calculations.....	92

Appendix B: Additional CFD Study Results.....	94
Appendix C: Component Material Certification	97

List of Tables

Table 1: Adhesion Wear Classifications	15
Table 2: Part Identification	37
Table 3: CFD Simulation Results	60
Table 4: Surface Finish.....	60
Table 5: 100% Lift Raw Data.....	94
Table 6: 75% Lift Raw Data.....	94
Table 7: 50% Lift Raw Data.....	94
Table 8: 25% Lift Raw Data.....	95
Table 9: 5% Lift Raw Data.....	96

List of Figures

Figure 1: Galling on the piston portion of the PRV component as a result of chatter.	3
Figure 2: Galling on the bore portion of the PRV component as a result of chatter.	3
Figure 3: Apparent area of Contact (left) versus True Area of Contact (right).....	7
Figure 4: Wedge Formation (Hokkirigawa and Kato 1988)	13
Figure 5: Adhesion Wear Formations of Islands.....	16
Figure 6: Depiction of Asperity Interactions.....	17
Figure 7: Temperature Profile (Blok 193).....	28
Figure 8: Isotherms (Archard and Rowntree, The Temperature of Rubbing Bodes: Part 2, The Distribution of Temperatures 1988).....	32
Figure 9: Typical PRV Installed on a Pressure Vessel.....	35
Figure 10: Section view of a PRV	37
Figure 11: Force Diagram of PRV Disk.....	38
Figure 12: Huddling Chamber Example.....	39
Figure 13: Backpressure Forces on a PRV's Disk	41
Figure 14: Built-up Backpressure from Discharge Restriction	42
Figure 15: Inlet Pressure Loss Example	43
Figure 16: CFD Computational Domain	48
Figure 17: CFD Mesh.....	48
Figure 18: Initial Conditions of CFD Simulation.....	50
Figure 19: Test Set-Up	52
Figure 20: Disk Stem with LVDT Attachment	53
Figure 21: Data Acquisition System.....	54

Figure 22: Full Open Pressure and Flow Trajectories Profile Plot	58
Figure 23: Detailed View of Flow and Pressure Profiles	58
Figure 24: Pressure Profile of Disk	59
Figure 25: Initial Surface Condition of Disk	61
Figure 26: Low Severity Test Run	62
Figure 27: Low Severity Test Run Detailed View	62
Figure 28: Low Severity Wear on Disk.....	63
Figure 29: Medium Severity Test Run	64
Figure 30: Medium Severity Test Run Detail View.....	64
Figure 31: Medium Severity Wear on Disk	65
Figure 32: High Severity Test Run.....	66
Figure 33: High Severity Test Run Detail View	66
Figure 34: High Severity Wear on Disk.....	67
Figure 35: High Severity Wear on Adjustment Screw	67
Figure 36: Disk Position and Pressure Difference Relationship	68
Figure 37: Galling of Component.....	83
Figure 38: PRV's Specification Sheet.....	92
Figure 39: PRV's Sizing Calculations Sheet	93
Figure 40: 75% Lift Pressure and Flow Profiles	94
Figure 41: 50% Lift Pressure and Flow Profiles	95
Figure 42: 25% Lift Pressure and Flow Profiles	95
Figure 43: 5% Lift Pressure and Flow Profiles	96
Figure 44: Material Composition of Disk Stem	97

Figure 45: Material Composition of Adjustment Screw 98

Abstract

This study was done to examine the mechanisms involved in the galling of stainless steel surfaces which are subjected to low static contact loads while undergoing a high number of sliding cycles. Presented is a theoretical explanation of why severe adhesion wear may exist in similar applications. The conclusions drawn are based upon other studies as well as the results of physical testing conducted. The testing involved sliding-fit components within a pressure relief valve subjected to high-frequency motion. Flash temperature, surface velocity, oscillatory motion, material properties, and oxide film are theorized to be the causing mechanisms of catastrophic adhesion wear when the normal loading is light.

Chapter 1: Purpose of Study

The overall intent of this paper was to develop knowledge in the area of adhesive wear occurrence in a special application. The application focused on high nickel alloy metals that were subjected to a high frequency sliding interaction with a small normal load applied. What made this a special application is the fact that a small normal load existed which resulted in a low amount of frictional force between the rubbing surfaces yet it is known that low frictional forces generally do not normally cause conditions for galling to happen. It was observed however that galling did occur in an application in which the rubbing surfaces moved at a high surface speed with low static contact load. The purpose of this work is to explore the mechanisms of why this occurred.

High nickel alloy metals such as austenitic stainless steels are used in a variety of mechanical applications because they have suitable and practical properties. These properties include several features: a resistance to oxidation, a resistance to chemical embrittlement, an acceptable strength, and an ability to be easily machined or formed into functioning components. An inherently non-constructive property this type of metal has is its high susceptibility to gall and furthermore it is known that austenitic stainless steels have poor wear characteristics in a sliding application (Hsu, Ahn and Rigney 1980). Galling is a type of adhesive wear in which material is relocated from one surface to another by solid-phase welding material (Hamrock, Schmid and Jacobson 2005). Galling is a term characterized as macro level adhesion wear in which a human eye is able to observe direct material transfer and surface finish degradation.

When galling occurs, the surfaces which were initially “smooth” become rough and marred. This wear leads to a distortion of the shape and an increase in the frictional forces between the two surfaces. A malfunction is likely to transpire if the mechanical system’s function is dependent on the two surfaces' ability to guide another part or are required to have a low friction sliding fit.

Such a mechanical system with these critical mechanical functions exists in the realm of pressure relief valves (PRV) which was the primary case study of this thesis. It is a known concept in the PRV industry that high cycle oscillations of a PRV will be destructive and can lead to friction welding of components (Smith, Burgess and Powers 2011). Figure 1 and Figure 2 displays the result of this movement, otherwise known as chatter, on a PRV's components. This presented a real world application which helped this work by providing an example and proof of the existence of galling in a low static contact situation.

PRVs have a system of components which guide a “face seal” style of seal from a closed to open position when actuated. It is critical that the seat have guiding so that a good seal is ensured each time the PRV opens and re-closes. Furthermore it is important that when the guiding components, slide against each other, there is not a large amount of frictional resistance, otherwise the general action of the PRV may be restricted and not function as it was intended.



Figure 1: Galling on the piston portion of the PRV component as a result of chatter.

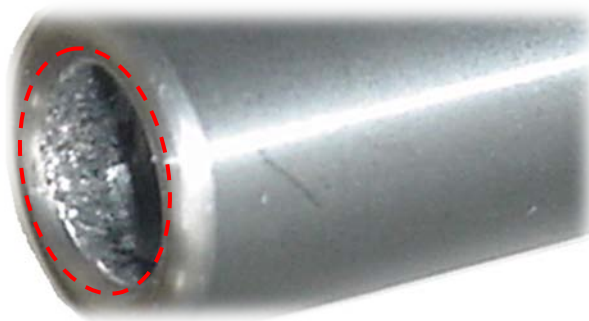


Figure 2: Galling on the bore portion of the PRV component as a result of chatter.

These guiding components may be described as a bore and piston style mechanism in which the piston is the moving part and the bore is stationary while guiding the movement. The fit class between these parts is loose with 0.004 inch (0.10 mm) to 0.017 inch (0.43 mm) of clearance. Since the guiding surfaces will come into contact, friction does exist, but it is relatively small because there is not a great amount of contact side load on the guiding surfaces. With low contact loads, stainless steel components are not likely to gall and a PRV can perform a number of times without any functional issues. The assumption for estimating a long service life is that the PRV's components open and close once per actuation of the valve. If however a PRV is installed onto an application which causes flow instabilities, a high cycle frequency actuation can exist; flow instabilities will cause a PRV to open and close repeatedly

during a single relief event. The occurrence of galling has been observed in a number of cases where flow instabilities exist in PRV applications.

Wear in general may be characterized as being unpredictable (Flinn and Trojan 1975). The reasoning behind this characterization is due to the variables involved and the interdependencies they each carry. There are several known variables which influence the occurrence of adhesive wear: the materials and their properties, the static contact load conditions, the nature of the surfaces, and the lubrication between surfaces. Galling wear is classically found by relate the volume remove to the yield strength of the material to provide a prediction on the acceptable amount of normal loading the surfaces can undertake without generating wear. The volume (v) of a material removed by adhesive wear is directly proportional to the applied load (W), the sliding distance (L), and is inversely proportional to the hardness (H) (Hamrock, Schmid and Jacobson 2005). Using an adhesive wear coefficient (k), which is a function of various properties of the materials in contact, one can predict a wear life from the well accepted theory shown in Equation 1.

Equation 1

$$v = \frac{kWL}{3H}$$

Glaeser expands this model shown in Equation 1 slightly and pronounces that it is based on a few assumptions. The equation assumes that the wear occurs by shearing of the true contact area and that the true contact area is a result of the contact stress yield point of the weaker surface. Also assumed is that wear is proportional to the total sliding distance. The expanded equation is shown in Equation 2 where P_m is the indentation yield point.

Equation 2

$$v = \frac{kWL}{P_m}$$

By these mathematical models, wear is proportional to the load and sliding distance while it is inversely proportional to the hardness of the weaker material. The wear coefficient is essentially a measure of the probability that each asperity contact produces wear volumes of material. This value has to be derived experimentally and is assumed to be constant in value. It is the authors opinion that, though these equations may give general predictions for large loads, it is oversimplified since the surface and contact area are likely to change and there are other components at work during the wear process. Additionally, these equations assume that sliding speed is slow and singular and a temperature component is not considered. For these reason Equation 1 and Equation 2 cannot be applied towards all galling problems, especially for the case examined in this work.

One situation of galling wear not as understood is when the normal applied static load is relatively low and the movement between the surfaces is a fast oscillatory motion. It was suspected that the frequency of movement is a key factor in galling as a result of a localized temperature increase from friction among the surfaces.

The research presented in this paper helped fill a knowledge gap in the area of galling wear since a direct examination of galling in a low static contact and high cycle movement was done. The study in this paper was important also because it may be directly applied towards PRVs. Those that will benefit from this work include PRV discharge system designs or more generally those who are designing a mechanical system with high nickel alloy components with sliding fits.

Chapter 2: Theory and Literature Review

Before moving forward into the research of the mechanisms involved in this special case of galling, some general background research was done to help understand the problem. Galling, which is also described as catastrophic adhesion wear, was explored to understand the basic concepts and help generate questions and speculations later for the special case. Overall PRV mechanical functions were examined as well as its applications in which high frequency movement occurred. This provided a better understanding of why flow instability exists. This background information may help the reader gain a stronger grasp of the issue and also help broaden their knowledge of PRVs.

Friction

In order for any form of wear to occur, friction between surfaces must be present to cause plastic deformation and heat generation. Because of this fact, it was important to first discuss and understand the theory of friction. The case considered in regards to friction and this work was that the sliding interaction was not lubricated. Lubrication greatly affects the amount of frictional force between two sliding surfaces and actually inhibit galling. However, due to the nature of the type of application this work focused on, lubrication was not practical and was not a viable aspect to consider. The sliding nature between two surfaces is dictated by the frictional forces between them. Frictional force is influenced by each of the surfaces' tribological aspects and material properties.

Regarding to the tribologic notion, surfaces are naturally unsmooth and have a level of roughness caused from the existence of asperities. Asperities are the microscopic roughness or “peaks” on the surface of a material. They are fundamentally

unavoidable in machining or other forming processes; even a well-polished surface will have inhomogeneities. There are several reasons why asperities on a surface can exist: scratches and pits caused from machining and forming processes, variations in the physical grain orientation in the nature of phases and inclusions, and even differing microstructures and hardness (Flinn and Trojan 1975). The severity of these asperities influence friction between surfaces. Furthermore, surfaces contact one another only at these peaks of the asperities. The contact area created by touching peaks is referred to as the real or true area of contact rather than the apparent area of contact. Figure 3 provides a depiction of the differences between the apparent area and true area of contact; the areas are highlighted in yellow. One can observe that at the microscopic scale that the true area of contact is in fact at the peaks of the asperities rather than the projected area of the object.

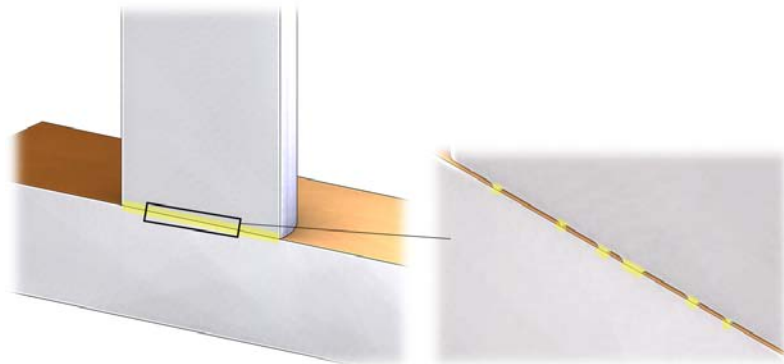


Figure 3: Apparent area of Contact (left) versus True Area of Contact (right)

Coulomb and Amonton have created two laws regarding to frictional forces. The first is that the frictional force is independent of the apparent area between two surfaces. This is because the real area of contact is very small when it is compared against the apparent area (Bowden, Moore and Tabor, *The Ploughing and Adhesion of Sliding*

Metals 1942). The second law created states that the frictional force is proportional to the applied load. This is because the area of real contact gets larger as normal load increases from the result of plastic flow (Bowden, Moore and Tabor, The Ploughing and Adhesion of Sliding Metals 1942). This is due to the fact that the pressure generated on the real contact area is exceptionally high even under small applied loads (Markov and Kelly 1999). The pressure generated causes the plastic flow until the contact area is great enough to support the load. The real area of contact is proportional to the normal load (W) but inversely proportional to the hardness (H); this is shown by Equation 3.

Equation 3

$$A_{true} = W/H$$

The real contact area influences electrical conductivity, thermal conductivity, optical phenomena, and friction and wear (Glaeser 1971).

Friction primarily exist as a result of two concepts. One is the shearing of metallic junctions which were formed by adhesion at the area of real contact (Bowden, Moore and Tabor, The Ploughing and Adhesion of Sliding Metals 1942). The surfaces "stick" to each other. The second is that during sliding, the asperities of the two surfaces are physical riding against each other and work has to be done to either displace one of the surfaces or shear off one of the asperities. A surface's material properties have a large influence in both of the ideas behind friction. The materials crystal structure, surface finish, and surface composition all influence the asperity geometry; otherwise known as the microscopic surface profile. In this case, friction is a function of only the hardness and the shear strength of contact junctions (Glaeser 1971). The material's hardness and cohesive bond strength influence the adhesion force and the allowable

shear stress of the asperities; this is essentially how easy the asperities break apart during collisions.

The frictional force is calculated by Equation 4 in which the total frictional force (F) is the addition of the required shear force (S) to break the metallic junctions and the force (P) required to displace the non-shearing asperities caused by the relative surface roughness. Friction is naturally higher on very rough and interlocking surfaces because of high points and increase in displacement force. (Glaeser 1971).

Equation 4

$$F = S + P$$

This equation can be expanded slightly by relating it to the true area of contact as shown in Equation 5. The required shear force is the force needed to break all the asperity interferences of both surfaces which is equal to the product of the true area of contact (A_{true}) and shear strength (s) of the junction interface.

Equation 5

$$F = sA_{true} + P$$

If Equation 3 and Equation 5 are combined, one can explain the force of friction further as shown in Equation 6.

Equation 6

$$F = \frac{sW}{H} + P$$

If the macro surface roughness is omitted and the force required to displace junctions P is eliminated, then the coefficient of friction can be determined by Equation 7.

Equation 7

$$F = \frac{sW}{H} \rightarrow \frac{F}{W} = \frac{s}{H}$$

where $\frac{F}{W} = \mu$ coefficient of friction

The coefficient of friction is a useful concept for determining the force of friction when the normal load is known. As Equation 7 depicts, the coefficient is proportional to the shear strength of the junction and inversely proportional to the hardness of the two particular materials that are sliding. Relating this with wear, one can see that rubbing materials that have a high hardness and low shear strength will have a low friction force.

As mentioned earlier in this section, there are other factors involved in friction and the coefficient of friction cannot totally be used to determine friction force though it can be used as a close approximation. Surfaces with a great roughness will exhibit high friction, likewise very smooth surfaces will also have high amounts of friction. In the smooth surfaces however, it is the surface tension forces that become significant in the high friction forces. This is because surfaces of the same material will naturally stick to one another because of bonding. This bonding exists in surfaces with little foreign contaminants and has been proven in studies with metals of highly cleaned surfaces in a high vacuum environment. The surfaces may be stationary or moving. It is known that even for low speeds and stationary contacting surfaces, adhesion and welding will occur at the contact points (Bowden, Moore and Tabor, *The Ploughing and Adhesion of Sliding Metals* 1942). Further investigation of the aspects in determining the frictional force is beyond the scope of this work; the inner workings of friction needed to be established only.

In all cases of friction, frictional heating exists to some extent. Frictional heating causes softening of the surface layers and degradation of oxide films which results in pure/clean contacting surfaces and adhesion (Glaeser 1971).

Wear Mechanisms

There are several different types of wear and the main topic of wear in this paper was adhesion wear, however the other forms were worth noting in order to establish the differences among them. The types are adhesive, abrasive, and chemical wear.

Chemical wear is when corrosion of a surface occurs and produces fracture of the surface under high contact stress. Chemical wear is not considered in this work.

Abrasive wear is general scratching of a surface with an absence of any bulk material being transferred between surfaces. Abrasive wear was not a topic of this work and any elaboration about it is beyond the realm of this work. A simple idea of distinguishing abrasive wear against adhesive wear is that abrasive wear is associated with surfaces while adhesive wear is associated with volumes. In all forms of wear, a surface is highly stressed at contact points where either shearing, fracturing, or plastic deformation takes place and parts of the surfaces are separated and become debris (Glaeser 1971).

Adhesion wear is however the primary focus of this thesis.

Adhesion wear is classified in this work as microscopic transfer of metals to another surface; the surfaces are not necessarily critically ruined and cannot be seen by the human eye. Adhesion is synonymous with welding, sticking, or as material transfer and these terms are used throughout this paper interchangeably. Most sliding surface will have some amount of adhesion wear but the surfaces may not be ruined. The key distinction between general adhesion wear and the four forms of "severe" adhesion wear that are discussed in this work is that severe adhesion is at the macroscopic level and visible by the human eye. The term severe is used to distinguish a high severity level of adhesion wear.

Considering the initial stages of adhesive wear, it cannot begin without some form of abrasive wear initially (Markov and Kelly 1999). The exact mode of material transfer is likely to change from the initiation up to the point of being considered catastrophic or severe. Adhesive wear is common in dry contact conditions with metals that have about the same hardness (Glaeser 1971).

Markov and Kelly classify adhesion wear into two main types, low-energy and high-energy. Low-energy refers to relatively slow sliding speeds while high-energy refers to fast sliding speeds. Low-energy includes two subtypes which are seizure and scoring while high-energy subtypes are scuffing and galling.

Seizure is caused by plastic deformation of only one surface at slow sliding speeds and travel only a small amount of distance. Hardened metal fragments are transferred onto the harder surface from the softer surface as a result of the protrusions on the hard surface plowing and widening grooves on the soft surface. This is not a product of temperature hence the slow speed classification criteria. What happens is the fragments, created by normal abrasive wear, cause an increase in the local pressure and increase the inclination for additional plastic flow and work-hardening. Hardened fragments are stronger than their initial bulk body and thus escalate the fragmentation of the bulk body which produces more and more wear.

Scoring is best described as plastic deformation of both surfaces without the formation of adhesive material transfer. It results in the formation of macroscopically visible grooves and scratches in the direction of sliding (ASTM 2015). During scoring, two mechanically interlocked "wedges" from both surfaces are created from the plowing of the two sliding metals which are a result of work-hardening on either

surfaces. Here a wedge refers to a formation at the leading edge of a sliding body which was resulted from plastic flow of a bulk material. This form of adhesion wear is likely to occur when a developed wedge has a hardness greater than the hardness of the opposing surface and has a slow sliding speed (Markov and Kelly 1999). The second wedge ends up being softer and get sheared and transfers to the surface of the harder wedge. Continuous plastic deformation in regards to sliding surfaces can be describes by a wedge formation on the weaker surface. This occurs as a result of a friction force "pulling" the weaker material along with the other surface. See Figure 4 for a depiction of the referenced wedge formations. As discussed in a prior section of this paper, the friction force is a result of asperity collisions and local bonding. Any geometric defect on the surface, but not necessarily contaminates, will only aid to initiate the process sooner because it increases the friction force.

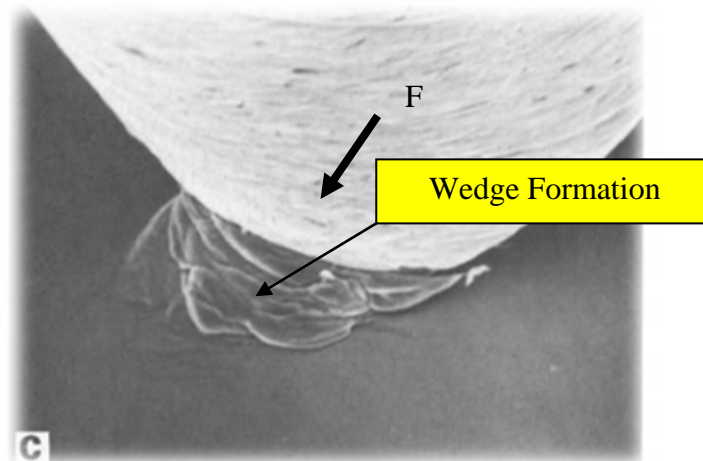


Figure 4: Wedge Formation (Hokkirigawa and Kato 1988)

Markov and Kelly define the transition from low-energy to high-energy adhesion wear when the sliding speed reaches a critical value which causes the surface

temperature to rise significantly and the mechanisms of plastic deformation to be related to temperature rather than shear stress alone.

Scuffing and galling are high-energy modes of wear classified as severe adhesion wear because material from one surface is transferred and sticks to another surface as a result of heating and softening of the metal surfaces; heat is generated from the frictional rubbing. These are considered to be high-energy adhesion wear types due to the temperature dependency definition. ASTM standard G40-15 defines scuffing as "a form of wear occurring in inadequately lubricated tribosystems that is characterized by macroscopically-observable changes in surface texture, with features related to the direction of relative motion." Furthermore ASTM G40-15 defines galling as "a form of surface damage arising between sliding solids, distinguished by macroscopic, usually localized, roughening, and the creation of protrusions above the original surface; it is characterized by plastic flow and may involve material transfer." By these definitions, scuffing and galling are in general accord with each other as far as descriptions, however scuffing may be better grouped with the idea that a wedge formation occurs while galling may or may not have any existence of wedge. During scuffing the fragments which are transferred are in the wedges. Scuffing is normally preceded by scoring (Markov and Kelly 1999). The main difference between scuffing and scoring is that the rise in surface temperature cause the plastic flow and fracture.

By ASTM's definition, galling may include wedges but it is the author's opinion that galling is better described as being related with the collision and fracture of surface asperities rather than the formation and breakage of wedges. This is mostly because the author has seen evidence of this form of severe adhesion wear in the application of two

sliding surfaces with a very low normal load; the lack of a high normal load means that large plastic flow and thus wedge formation is unlikely. This agrees with Markov and Kelly's assessment that galling is caused by the plowing of a soft surface by hard asperity peaks. The plastic deformation rate of a metals surface layer is so great that the fragmented surface metals flow as a gum and do not harden, by means of tempering, during the deformation so wedge growth is not possible (Markov and Kelly 1999).

Table 1 describes the classification criteria for the energy subtypes of adhesion wear.

Table 1: Adhesion Wear Classifications

Adhesion Wear Classifications Criteria				
Energy Type	Speed Criteria	Sub-Type	Hardness Criteria	Temperature Criteria
Low Energy	<0.4 to 0.7 m/s	Seizure	Wedge $H < \text{Surface } H$	
		Scoring	$\text{Surface}_1 H > \text{Surface}_2 H$	
High Energy	>0.4 to 0.7 m/s	Scuffing		Surface $T > \text{Crystallization } T$
		Galling		Surface $T < \text{Crystallization } T$

H is hardness and *T* is temperature
(Markov and Kelly 1999)

Indications of galling are scattered "islands" of transferred metal on the surface however if galling continues, the islands will form into a fully connected plate of transferred metal. See Figure 5 below. These layers are essentially smeared onto the opposing surface and have the potential to build on top of one another. The thickness of these islands may range from 0.06 to 0.1 mm [0.002 to 0.004 in] and depend on the total applied load (Markov and Kelly 1999). The transferred material in a galling type of wear will adhere to the surface of greater hardness and as buildup of layers continues, the pressure and thus friction locations get redistributed which explains the random scattering of the islands. As the sliding surfaces continue to cycle in movement, the

volume of transferred metal grows larger as the friction force of the surfaces gets larger. The islands created have the potential to be work-hardened during the adhesion and recrystallization process. This means that once islands of transferred material form, the subsequent wear mechanisms may include scoring as well as continued galling.

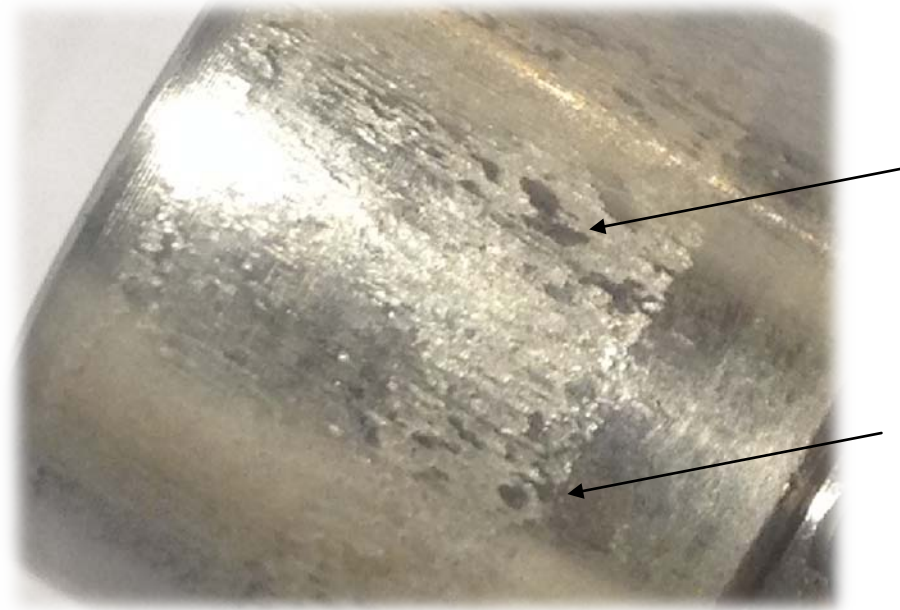


Figure 5: Adhesion Wear Formations of Islands

Galling is a type of high-energy wear in which there is a large concentration of energy which causes metal to change in properties and flow as amorphous material (Markov and Kelly 1999); amorphous flow is essentially dislocationless deformation. These researchers also state that all high-energy types of adhesion wear are accompanied with amorphous modes of plastic deformation. The source of this high concentration of energy is produced from asperities between the surfaces sliding against each other which generate high stresses and plastic flow in the areas of contact. Figure 6 is shown to help illustrate the interactions between the asperities as two surfaces slide against each other.

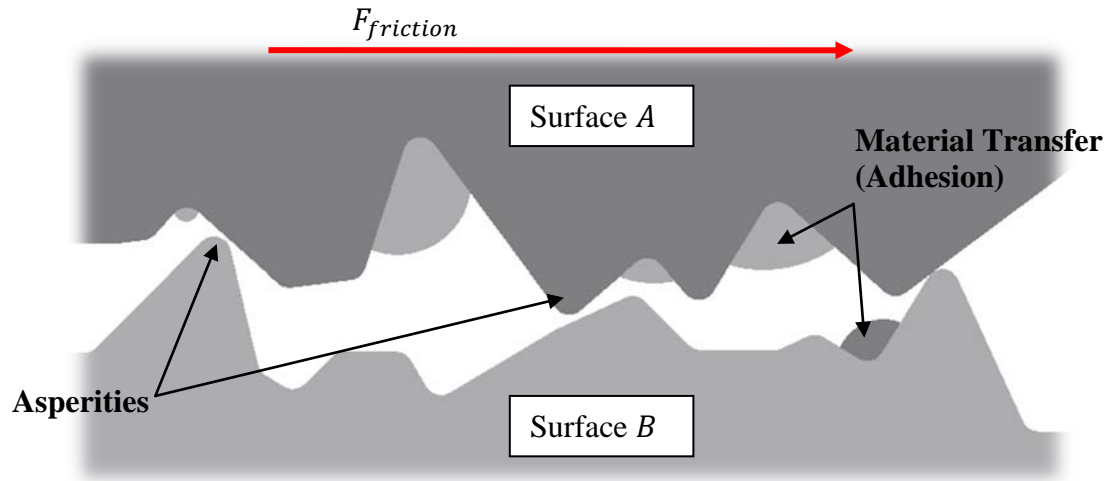


Figure 6: Depiction of Asperity Interactions

The peak of greater hardness will plow through the softer surface's peaks as the surfaces slide against each other; fragments of the softer surface are left stuck to the harder surface. Material transfer and adhesion occurs when the adhesion strength of an asperity is great enough to shear an opposing asperity (Bowden, Moore and Tabor, *The Ploughing and Adhesion of Sliding Metals* 1942). Adhesion energy is the amount of energy per unit area to break an asperity interface into two surfaces. When an asperity located on one surface plows into asperity of the opposing surface and shears it from its initial substrate, fusion of the broken asperity to the other surface will occur. An asperity breaks off as a result of the applied stress being greater than its maximum shear stress. When the shear stress is not substantial enough to overcome the adhesion strength and break apart an asperity, the surfaces will simply follow each other's profile without any material transfer or breakages. An analogy to when asperities do not shear but still attribute to the friction force is when two bristled brush being rubbed against another. The individual bristles are the asperities and they deflect against one another but do not break. Work has to be done to move the brushes which is the friction force.

In this case the energy is not great enough the cause breakage of the bristles since the bristles have a greater shear strength than what is being applied.

When breakages do occur, the broken pieces may either be rejected in the form of fine particulates, or they may potentially stick to either of the two sliding surfaces. A welded junction is formed at the location of the ejected asperity reattaching to a bulk surface. Welding is only achieved when re-crystallization temperatures are accomplished (Markov and Kelly 1999). With the increase in temperature, the broken off fragments melt and then solidify onto the cooler surface. This means that one key component which distinguishes adhesion wear against other types of wear is temperature, and more specifically the localized temperature at the initiation site on the surface layer.

The behavior of metal transfer is related to the relative strengths of the sliding surfaces and the adhesion strength of the transferred material to the opposing bulk surface. Morkov and Kelly attest that when the adhesion strength is weaker than either of the two metals, then the shear and thus material transfer is small. If the adhesion strength is weaker than one of the metals but stronger than the other, then shearing of the junction will occur on the soft, weaker metal and the direction of transfer is from the soft to the hard metal. In this case, the harder metal will show the signs of galling. If the junction strength is greater than the strength of one of the surfaces, then the material transfer direction is from the softer metal onto the harder metal with some partial transfer in the opposite direction. In this case, both surfaces will indicate signs of galling but the harder of the two metals will show it to a greater extent. The final scenario Morkov and Kelly describe is when the junction strength is stronger than the

strength of both sliding metals. When this is the case, both sides exhibit shearing of asperities and there is a work-hardening of the surfaces. Both sides will show signs of galling.

At the initial stages of adhesion wear, discrete metallic fragments begin to transfer and weld to a surface. The weld growth is dependent upon several items including the sliding distance and amount of interface separation which is related to the adhesion strength (Chen and Rigney 1990). The amount of adhesion strength is able to be calculated in order to predict when galling between metals may occur by first making a few assumptions to simplify the equation. Using the assumption that all asperity interfaces prior to shear are treated as large-angle grain boundaries, one can determine the adhesion energy for a metal by using Equation 8 where γ_A is the surface energy of metal *A* (Chen and Rigney 1990). Surface energy is basically molecular attraction forces. The equation assumes that the metal is a single-phase binary alloy which essentially means that mixing of surface materials has not occurred and the surfaces are “pure” in the sense that foreign metals do not exist upon the surface. This also uses an approximation that the grain boundary energy is one third of the surface energy (Seah 1976).

Equation 8

$$\Delta E_A = \frac{5}{3}\gamma_A$$

The direction of the material transfer between two surfaces can be determined by examining the surface energies of each metal surface. Consider a metal surface *A* sliding against a metal surface *B*. Making the assumptions that during a sliding event the surfaces are free of foreign particles, there is no solute redistribution, and mixing or

chemical change do not occur, one can predict that the if $\Delta E_A - \Delta E_B$ is a positive value, then metal surface A will be transferred to metal surface B according to Chen and Rigney. If the aforementioned equation takes a negative value, then the transfer direction is reversed and metal surface B is transferred to metal surface A . Thus the required energy change in a metal transfer event from surface A to surface B can be determined by Equation 9 (Chen and Rigney 1990). Here ΔE_{AA} and ΔE_{BB} indicate the cohesive strength of each metal surface; it is essentially how well the metal sticks to itself. From that, one can observe that the cohesively weaker metal will transfer to the stronger metal surface.

Equation 9

$$\Delta E(A \rightarrow B) - \Delta E(B \rightarrow A) = \Delta E_{AA} - \Delta E_{BB} = \frac{5}{3}(\gamma_A - \gamma_B)$$

This equation should be recognized as a general rule of thumb for indicating direction of material transfer during adhesion wear and that it is a simplified model. In actuality the model should consider the solute fraction on a grain boundary and the enthalpy of mixing the two surfaces. Chen and Rigney consider these aspects as well as created an interaction parameter of the asperity junction. The complexity of the actual event however is beyond the scope of this work.

Equation 9 presents the question of "what if the two sliding surfaces are of identical material in regards to physical properties and chemical composition?" It was suspected and shown through physical testing that both surfaces show signs of adhesion wear when they are of the same material composition. This occurrence can be explained by the randomness of asperity breakages and an approximation that both surfaces have the same strength.

Galling and other forms of adhesion wear can be avoided by the utilization of dissimilar metals because dissimilar materials are less likely to be attracted to one another. Additionally, the usage of hard or high strength materials can be done to reduce galling. However, it is possible to still have a high wear rate and also a resistance to galling, or to have a low wear rate and high galling tendencies; it has to do with surface hardness and bulk material properties (Hsu, Ahn and Rigney 1980). The asperity may simply break off but not stick. This would be brittle fracture of the surface which is typical of abrasive wear. Similarly, since adhesion is associated with plastic strain, a stronger material would be less likely to deform and adhere to a surface.

Metallurgy

The metallurgical aspect has a large bearing on the mechanisms of galling in this work's case study. Plastic deformation of a metal has an influence on wear mechanisms and its characteristics are dependent on the details of the material's microstructure (Hsu, Ahn and Rigney 1980). For this reason and because austenitic stainless steel components were used in the case study, it was critical to develop an understanding of the material properties. Furthermore it has been established that the relative hardness of a metal's surface will influence its inclination to gall. This level of inclination mostly depends on the immediate surface properties.

The unit cell of the crystal structure of austenitic stainless steels is a face-centered-cubic arrangement which have a large number of slip planes. Between unit cells and along the slip planes are interruptions called stacking faults. Stacking faults are essentially defect properties intrinsic to a metal's crystal structure. At each of these faults there is a certain amount of energy that will cause the cells to dislocate and slip.

The amount of force required to do this is called a stacking fault energy (LeMay 1981). This is an inherent property of the material because it depends on the bond type and direction of the slip plane. This is important to note because there is a strong relationship between wear resistance and stacking fault energy; a high stacking fault energy results in reduced wear resistance. This work focused on 316 stainless steel which has a high stacking fault energy equal to about 80 mJm^{-2} (Hsu, Ahn and Rigney 1980). Alloy 316, and many other grades of stainless steel, has a high nickel content. It has been established by Schramm and Reed that as the nickel content rises, one can expect an increase in the stacking fault energy. Nickel elements within the metal structure influence the dislocation cross slip that can occur when the material is loaded; nickel raises stacking fault energy. Thus, high nickel alloys exhibit a cell structure of dislocation in the face-center-cubic structure which enables easy cross slippages (Schramm and Reed 1975). However, concentrations greater than 20% of nickel in an alloy will have diminishing effects on stacking fault energy values. Chromium elements within the crystal structure also have an influence on the stacking faults of stainless steel alloys but to a lesser extent. An increase in chromium content will cause the dislocation arrays to become planer which reduces stacking faults but only to a concentration up to about 15-20%. A greater concentration will have diminishing effects on the stacking faults (Schramm and Reed 1975). The existence and lack of existence of other elements will have an effect on the stacking fault energy but to lesser extents than chromium and nickel.

Materials with a low stacking fault energy will have better wear resistance than materials with high stacking fault energy (Hsu, Ahn and Rigney 1980). This is because

a unit cells with high stacking fault energy will dislocate more readily than that of unit cell with a lower stacking fault energy. Stacking fault energy has a control over the dislocation cross slip and climb in a materials structure (Schramm and Reed 1975). This has bearing on a metal's work hardening and creep behavior as well as its susceptibility to stress corrosion cracking and hydrogen embrittlement. Metals with high stacking faults are not as prone to stress corrosion cracking. Even within general stainless steels, stacking fault energy values will vary greatly because the values depend on the exact composition. In a face-centered-cubic arrangement, the stacking faults occur at the close-packed planes.

Schramm and Reed describe a method for determining the stacking fault energy of a material by relating stacking fault probability and other characteristic properties of a material, however that is not within the scope of this work. What is important to this work is how stacking fault energy is related to the occurrence of wear and most specifically adhesion wear. Consider a wear scenario in which a high stacking fault energy material's surfaces slide against another surface. A unit cell located at the outer layer of the surface has a large shear strain applied and due to its ease of dislocation, the cell layer fractures because of its inability to support the stress. This ease of dislocation relates with the ease of wear to occur. For this reason, stacking fault energy has a direct relationship with the surface hardness.

Hard materials are generally known to be wear resistant; this is largely because the unit cells are able to support high stress with little deformation and thus have a low stacking fault energy. It has been established that hard metals are used to reduce the inclination to gall because they possess a greater strength. This means that larger

amounts of forces are required to break off asperities to cause fragmentation. The ductility of an asperity has an influence on the adhesion effects. Low adhesion is seen in low ductile asperities which correlates well with high strength metals being resistive to adhesion wear; conversely hard metals are prone to stress corrosion cracking.

Austenitic stainless steels however, which are known to be soft and of lower strength, likely to undergo a martensitic transformation when it undergoes plastic strain at normal working temperatures. This is known as work-hardening. This is because austenitic stainless steels are typically metastable (Hsu, Ahn and Rigney 1980). During work-hardening, the surface of the material transforms from austenite, a face-centered-cubic structure, into martensite, a body-centered-cubic structure. Work-hardened surfaces can cause abrasive wear since it becomes a higher strength surface. When sliding occurs, an adhered material can be work-hardened and cause abrasive wear on the opposing surface (Karlsson 2012). According to Hsu et al. there are three possible types of transformation that can occur in austenitic stainless steels during a work hardening process all which depend on the amount of temperature and level of strain. The first is when the face-centered-cubic is transformed into a hexagonal close-packed structure. The second is when a face-centered-cubic is transformed into a hexagonal close-packed structure and then into a body-centered-cubic. And the last is when a face-centered-cubic is transformed directly into a body-centered-cubic. All of these transformations result in a change to the materials initial microstructure on its surface.

This is all worth noting because a martensite structure generally has a low stacking fault energy and thus not as susceptible to galling. However in the case of this paper's application, work-hardening was not likely to occur because the surfaces are not

exposed to high amounts of plastic strain. This allowed the author to omit this aspect in terms of speculating galling behavior in the special application of this work.

The material's surface properties was an important aspect to consider during this work. Austenitic stainless steels have a natural tendency to passivate in a normal room temperature environment. Stainless steels form a surface layer which makes it generally un-reactive to various agents of corrosion. These metals have a thin film of hard chromium-oxide on top of a soft stainless alloy bulk material. This hard surface oxide layer undoubtedly has an influence on the overall wear characteristics and more specifically the propensity of adhesion wear to occur within sliding metals.

Surface contaminates along with oxide films reduce the adhesion of metals surfaces (Glaeser 1971). If two metallurgically identical surfaces were completely pure of films and contaminates, they would readily bond together (Bowden and Rowe, *The Adhesion of Clean Metals* 1956). Furthermore if the bulk material of sliding surfaces are fully isolated from one another by an oxide absorbed layer, the transfer of fragments would be absent (Bowden and Rowe, *The Adhesion of Clean Metals* 1956). However it has been postulated that stainless steels are more prone to adhesion because of the oxide surface which is very sticky (Hanson, et al. 2007).

If the surface has a high rate of fracture which is typical of a hard oxide surface, the wear rate, not necessarily adhesive wear, will be high. This is because the surface layer has high strength properties which make it inclined for brittle fracture. This is related but not directly correlated with adhesion wear. What may occur is that when a hard oxide layer fractures off and is removed from its substrate, a much softer material becomes exposed to the sliding interface. Hard oxide asperities from the opposing

surface are allowed to dig into the freshly removed oxide surface of the soft substrate. This enables material transfer and adhesion wear since the soft metal plastically deforms easily as the hard asperities induce large shear stresses.

Flash Temperature Concept

The primary mechanism of galling wear that this work focused on is the rise of temperature on the surfaces of rubbing metals. The energy dissipated by friction appears as heat and the temperature within the rubbing surfaces will rise an appreciable amount (Archard, The Temperature of Rubbing Surfaces 1958). According to Archard and Rowntree, flash temperature and phase-transformed materials have proven to have agreement in experimental studies. In these studies, it was shown that flash temperature induces the metallurgical phase transformation.

The concept of sharp temperature increases from friction was developed by H. Blok and is called "The Flash Temperature Concept." Flash temperature theory has been applied to scuffing problems in previous works. The flash temperature concept has also been useful in the field of lubrication and its relationship with lubricant breakdown. This concept can easily be described by using the metaphor of how a match stick is lit. A match head is pressed and rubbed against an abrasive surface prior to the match lighting. As the match slides against the abrasive surface, localized heat is generated from frictional forces at the match's head. When the heat generated causes the match's head to reach a temperature which equal to the phosphorus flashing temperature, ignition of the match head occurs. During this process, neither the abrasive surface nor the bulk of the match rise significantly in temperature.

The sharp increase of frictional heating, referred to as the flash temperature, is generated through the sliding action of the areas of contact between the rubbing surfaces. This area is assumed to be the location of the heat source and is a band-shaped along the surface. The production of heat is proportional to the sliding speed of the surfaces (Blok 193). The flash temperatures are concentrated on a surface layer in a very thin profile when compared to the overall width of the heat source area. As sliding speed increases, a narrower band and more localized, thinner in affected area, flash temperature is produced. When the speed is great enough, temperature will only be reached at points very close to the path of the heat source (Blok 193). The flash temperature concept however is limited to predicting the most immediate contacting surface temperature. This concept cannot be used to determine the temperature of layers below the surface.

Blok describes the temperature profile for a moving heat source which is shown in Figure 7. Here a two-dimensional cross section of the temperature distribution for the heat flux (q) shown moving along a surface with a speed (v) between two bodies. This profile assumes a uniform distribution of heat flux. It is shown that the maximum temperature rise (T_{max}) occurs between the middle and the trailing edge of the heat source.

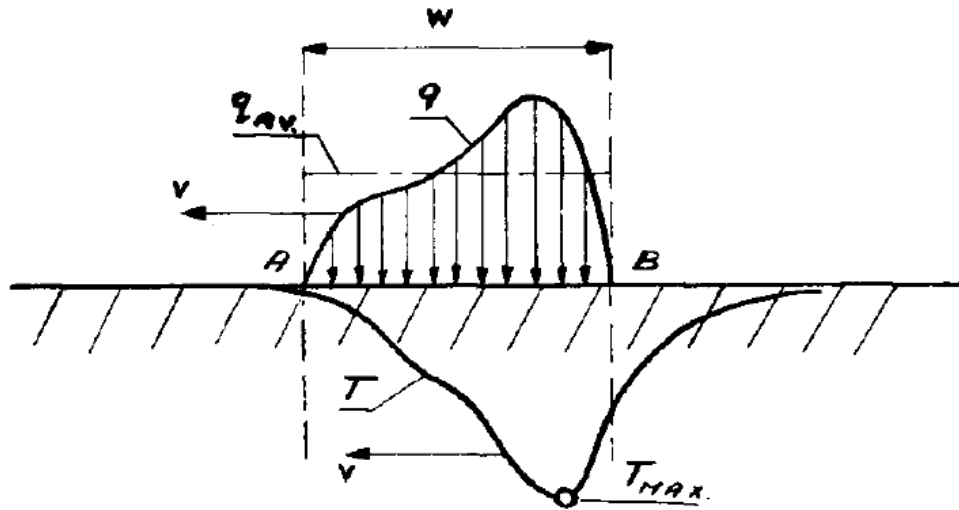


Figure 7: Temperature Profile (Blok 193)

The maximum temperature was important to the author as it can be applied to the incidence of severe adhesion wear and the onset of when galling occurs. Blok developed a mathematical model for predicting the highest temperature of a sliding body with a uniform heat flux moving at a uniform speed against a stationary body which is shown in Equation 10. Here the maximum flash temperature is equated to the product of several influential factors. According to Blok, Equation 10 is a good approximation for the maximum flash temperature when the sliding speed is high enough to cause the affected surface layer's temperature to be thin enough to produce a localized high temperature. In a slow sliding speed application, the bulk bodies may absorb the generated heat at a fast rate and the highly localized temperatures area not achieved.

Equation 10

$$T_{max} = A \frac{q_{av}}{b} \sqrt{\frac{w}{v}}$$

By this equation, the maximum flash temperature is directly proportional to the amount of heat flux but it also carries dependencies on the speed and width of the heat source. Here the width of the heat source (w) and the heat source's velocity are used to relate with the maximum heat source. The thermal contact coefficient (b) is used to relate the heat absorption properties of the material and is described by Equation 11. The variable c' is specific heat per unit volume and k is the heat conductivity. The specific heat per unit volume is simply found by multiplying the specific heat by the density of the material.

Equation 11

$$b = \sqrt{c'k}$$

The factor A is a form factor which is related to the heat flux distribution over the width of the heat source. For a uniform distribution, the form factor equates to $2/\sqrt{\pi} = 1.13$ while a semi-elliptical heat flux distribution equals 1.11; these two values seem to be true for a fairly smooth surface (Blok 193). The final component to Equation 11 is the heat flux (q). The heat flux is the energy generated from friction according to Hertz's theory of elastic contact. The maximum flash temperature occurs when the highest load possible is concentrated on the smallest area possible which is a result of plastic deformation (Archard, The Temperature of Rubbing Surfaces 1958). The realistic temperature of the two rubbing bodies is complex and difficult to pinpoint with total certainty is because heat is also being absorbed by the two bodies.

Archard extends flash temperature theory with more practical and physical considerations and attest that the distribution of the generated heat is dependent upon the level of speed. Assuming a circular area of rubbing contact, four characterizations

have been made for determining the mean temperature rise of a surface. The first scenario considers a stationary heat source. Heat is supplied between two bodies on a fixed area under steady state conditions. Archard describes that the mean temperature is able to be determined by Equation 12 where Q is the rate of heat supplied, a is the radius of the contact area, and K is the thermal conductivity of the body in question. This applies to low speeds and approximate equilibrium conditions of the stationary contact.

Equation 12

$$T_{mean} = \frac{Q}{4aK}$$

The next case considered is a slow moving heat source in which a moving body, identified as A, moves against a stationary body, identified as B. The velocity of A is slow enough that there is enough time for the temperature distributions to be established in A at each contact position; this is considered to be a steady state system. The mean temperature of the service is still represented by Equation 12.

The third case involved a speed criteria in which the moving body is moving fast enough so there is insufficient time for the temperatures distribution to be established as steady state within the stationary body B. The criteria for speed uses a dimensionless parameter (L) to relate the speed, area of contact, and the thermal diffusivity of the material. This parameter is given by Equation 13 where c is the specific heat of the body. Slow moving speeds are defined by Archard as $L < 0.1$ and high speeds as $L > 5.0$. For this third case, L is in between the aforementioned speed criteria.

Equation 13

$$L = \frac{Va}{2(K/\rho c)}$$

The last case identified is the fast moving heat source case where $L > 5$. In this case, the depth that the heat source penetrates the stationary body is small in comparison to the dimension of the contact area and thus any heat flow to the bulk of either rubbing body is negligible and the problem is treated as a linear heat flow (Archard, The Temperature of Rubbing Surfaces 1958). This is the case which this work focused on. In this condition, it is assumed that the supplied heat is constant to the surface and the temperature at the surface can be calculated by Equation 14 where q is the rate of heat per unit and t is the time duration for which the heat has been applied.

Equation 14

$$T = \frac{2q\sqrt{t}}{\sqrt{\pi K\rho c}}$$

Archard applies the point temperature to that of circular area of heat source contact and determined that the average temperature for a fast moving heat source can be determined by Equation 15. This equation relates the rate of heat supplied from the area (Q), the radius of the circular area of contact (a), and the thermal diffusivity (x) to determine the mean temperature generation. The thermal diffusivity is determined by Equation 16.

Equation 15

$$T_{mean} = \frac{0.31 Q}{K_c a} \sqrt{\left(\frac{x}{Va}\right)}$$

Equation 16

$$x = \frac{K}{\rho c}$$

Using the dimensionless parameter given in Equation 13 and the thermal diffusivity equation shown in Equation 16, the mean surface temperature of two rubbing bodies with a fast moving circular heat source, with $L > 5$, can be determined by Equation 17.

Equation 17

$$T_{mean} = 0.435 \frac{\pi q}{\rho c V} \sqrt{L}$$

This was determined by Archard from the data gathered by R. Holm. The primary assumption to all of the flash temperature concepts for a fast moving heat source is that all the heat is being supplied to the surface and isn't being distributed between the two bodies.

Examining the circular contact area, Archard and Rowntree deduced the isotherms of the flash temperatures. It was determined that the maximum flash temperature is located at the trailing edge of the area which agrees with what Blok had figured as well. Shown in Figure 8 are isotherms on a fast moving heat source contact area and was developed by Archard and Rowntree. It is seen here that the flash temperature value at various are represented as a ratio of the mean flash temperature.

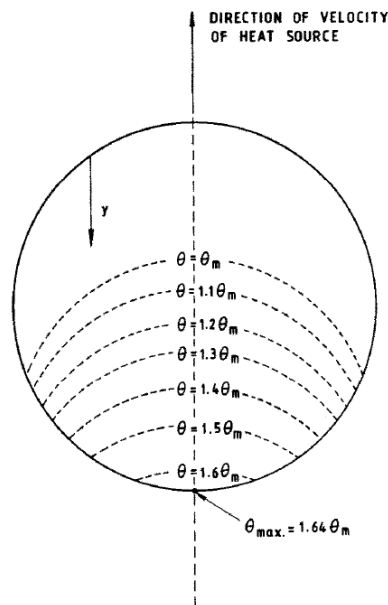


Figure 8: Isotherms (Archard and Rowntree, The Temperature of Rubbing Bodies: Part 2, The Distribution of Temperatures 1988)

The heat source in the flash temperature concept is supplied from the friction between the rubbing surfaces. The total rate of heat supplied is shown by Equation 18 where J is the mechanical equivalent of heat which is equal to a value of $4.17 J \cdot ^\circ\text{C}^{-1}$.

Equation 18

$$Q = \frac{\mu W g V}{J}$$

Comprehensively looking all of the flash temperature concept equations together, one can undoubtedly observe that the maximum attainable flash temperature is a function of the sliding speed. This is true even for situations where the applied load (W) is very small but still existent.

Archard points out in his works that surface films have a considerable effect on the temperature of rubbing bodies. He points out that oxide films have a low thermal conductivity which will raise the maximum flash temperature. The effects of a surface film will raise the surface temperature and will leave the temperature of the substrate unchanged (Archard, *The Temperature of Rubbing Surfaces* 1958). This will promote the occurrence of adhesion wear because as temperature increases, there is a decrease in strength and hardness and there is an increase in plasticity. At that point metal at the surface is encouraged to transfer to the other surface. This was important in this work's study since stainless steels have an oxide layer.

Temperature rise at the surface layers of two rubbing surfaces is a familiar concept, however its role in adhesion wear is less understood. Considering high-energy adhesion wear, the speed at which surfaces rub against one another can cause a pulse of high temperature rise in micro-volumes of a surface metal. A sharp increase in temperatures may lower the strength and increase the susceptibility of adhesion wear.

Pressure Relief Valves

PRVs were used as an investigatory means because it presented itself as a real world application aligned with the postulate of this work. This essentially gave this thesis evidence for the existence of galling occurring in a relatively low loaded sliding surfaces. When a PRV is subjected to a high frequency actuation, the associated mechanical loads can damage the valve and the result may be loss of overpressure protection, uncontrolled fluid release, and other potential hazards (Cremers, Friedel and Pallaks 2001). It was therefore prudent to research and gain knowledge about PRVs in general and investigate their applications in which the wear phenomenon has been identified to occur.

PRVs are used as a safety device on pressure vessels and pressurized systems. Figure 9 illustrates a typical PRV installed on a pressure vessel. The PRV sits atop the pressurized system and discharges into the atmosphere in the event of an overpressure. A PRV is a normally closed valve type and does not allow any media to pass through it. The pressurized media can be either a gas, a liquid, or as steam. A PRV has the purpose of protecting a pressurized system from exceeding a pressure threshold by providing a means for a controlled release of pressurized media once it is actuated and opened. There is an enormous amount of energy stored in pressurized media. A PRV stops the system from rupturing and releasing all the stored energy at once. A PRV is a self-actuated and completely mechanically controlled device used with a rationale of protecting lives and equipment. It is considered the last line of defense against catastrophic failure, meaning that once all other system controls, emergency shut-down features, or other safety mechanisms have failed to stop the overpressure, the PRV is the

final component to stop the unsafe condition of an overpressure. An overpressure is a pressure rise above a predetermined "safe" threshold pressure (Hellemans 2009). Once the PRV is actuated, it will release media at a given mass flow rate, then the system's pressure will drop back down to a safe operating level and the PRV will reclose. Once it recloses, no more media will be allowed to flow though.

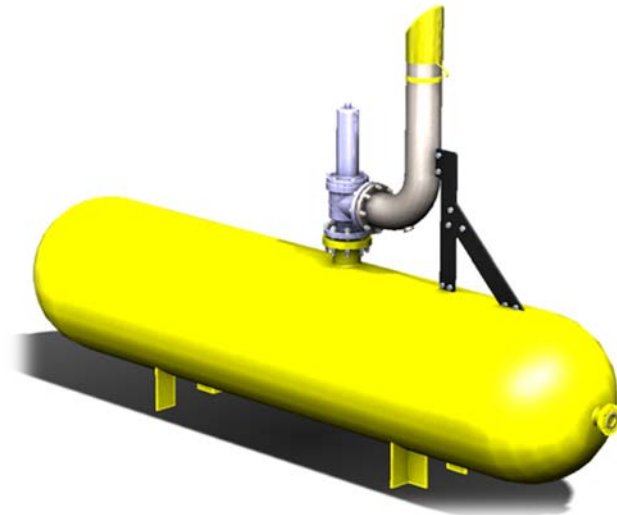


Figure 9: Typical PRV Installed on a Pressure Vessel

There are a number of scenarios which will cause a system to reach an overpressure and require a PRV. The details of these scenarios is not within the focus of this work, however what is relevant is that in the overpressure scenarios, there will be a required flow rate of fluid that the PRV will need to pass to prevent pressure from growing in excess. For this reason, PRVs come in many orifice sizes. The orifice of a PRV refers to the governing flow component within the PRV. The orifice of a PRV depends on the actual application and overpressure scenario, so there are multiple variations and configurations in which a PRV can be made. Not only does the orifice

size vary, but the required opening pressure and media phase will depend on the specific application as well. The focus of this work was on gas phase media.

There are subtypes which PRVs can be classified in. These types are pilot operated, conventional spring operated, bellows spring operated, and balanced piston spring operated PRVs (Hellemans 2009). Discussion of each subtype is not relevant towards this work other than the conventional spring operated. Conventional spring operated PRVs were used in the case study of this paper because will exhibit the high frequency cyclical movement which causes adhesion wear on sliding parts. The explanation for this happening first requires the understanding of how a conventional spring operated PRV works.

For ease of utility, refer to Figure 10 and Table 2 for PRV part identification and references. A conventional spring operated PRV functions entirely from a balance of force inputs. When a PRV is calibrated, the goal is to adjust it so that it opens at a predetermined pressure; this is also referred to as the set pressure. This is done by selecting a certain stiffness of spring for an associated orifice size and intended set pressure then installing it into a PRV. The spring is compressed and exerts a force in the closing direction. Following Hooke's Law, the springs force is equal to the spring's stiffness factor multiplied by the distance of compression. The spring force keeps the PRV closed during normal system operation by holding the disk against the PRV's seat which is located within the nozzle subassembly. The seat is the sealing element used to separate the inlet media from passing into the discharge space.

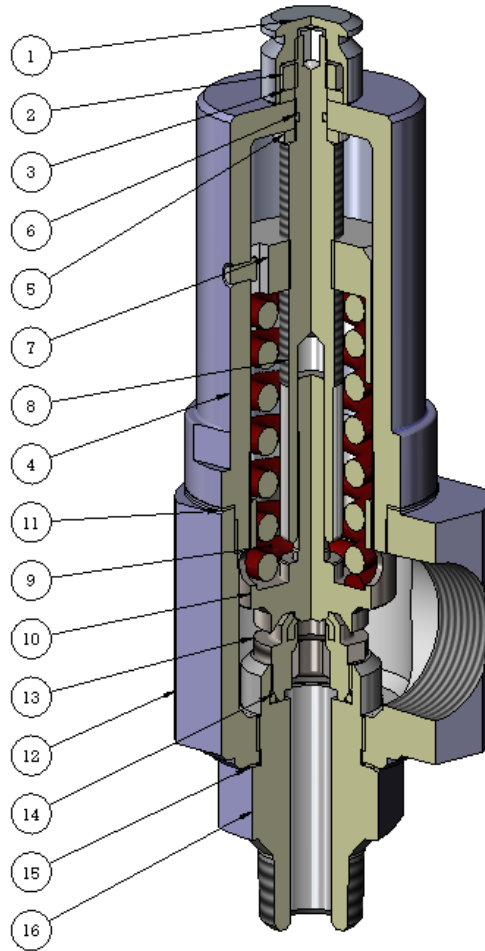


Figure 10: Section view of a PRV

Table 2: Part Identification

ITEM NO	PART NAME	ITEM NO	PART NAME
1	CAP	9	SET SPRING
2	LOCKNUT	10	DISK SUBASSEMBLY
3	LOCK WASHER	11	BONNET SEAL RING
4	BONNET	12	BODY
5	THRUST WASHER	13	NOZZLE
6	ADJUSTMENT SCREW O-RING	14	NOZZLE O-RING
7	ADJUSTMENT BUSHING	15	BASE SEAL RING
8	ADJUSTMENT SCREW	16	INLET BASE

The system's pressure generates a force component in the opposite direction to the spring force. This is a result of the pressure acting on the bottom surface area of the disk area; pressure multiplied by area is equal to the equivalent force. The entire surface area of the bottom of the disk is not exposed to the system's pressure when the PRV is closed, it is only the area within the seat's projected area. Figure 11 gives an illustration of the forces. Here, F_s is the spring force, F_v is the force generated by the pressure in the system. When the resultant force generated by the system's pressure is equal to that of the spring, the disk will begin to lift and remove the seal between the seat and disk. This occurs as the system's pressure approaches the set pressure of the PRV.

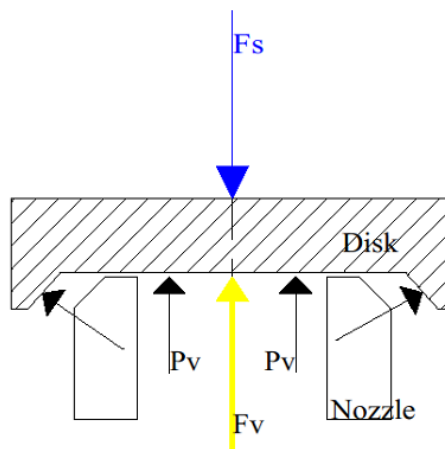


Figure 11: Force Diagram of PRV Disk

In order for the PRV to flow the media and relieve the overpressure, the disk must rise away from the nozzle a certain distance; this is referred to as lift. As the disk of the PRV lifts, the spring must be compressed further, thus generating additional force in the closing direction. In order for the PRV to lift, additional force must exist in the opening direction to overcome the spring force. The additional force is generated by the disks "huddling chamber." The huddling chamber is an annular pressure space located between the nozzle and the disk for the purpose of generating a rapid opening

(Hellemans 2009). Shown in Figure 12 is an example of a huddling chamber profile. The huddling chamber is designed to allow the media to create the additional lifting force on the disk.

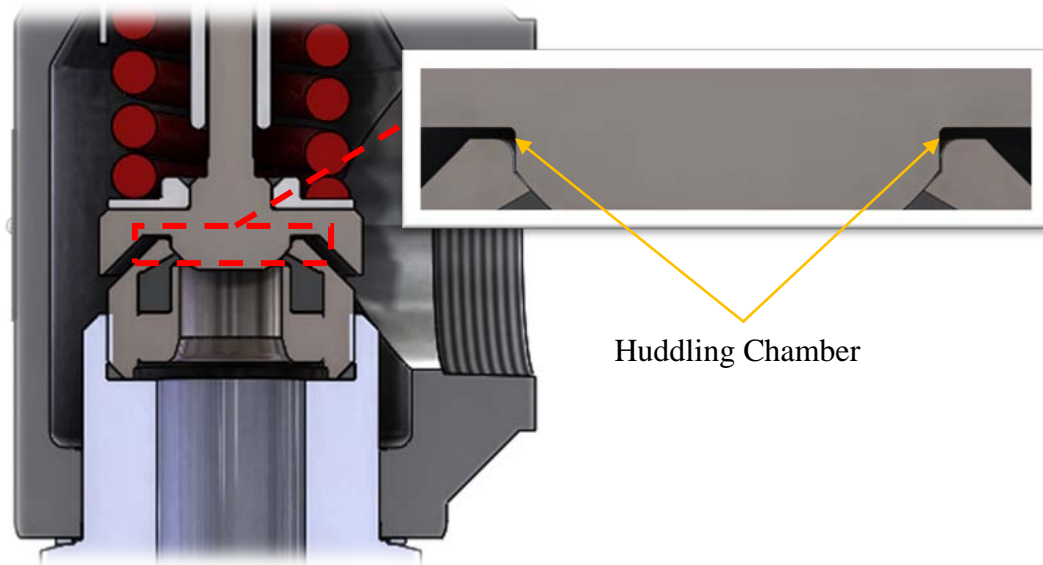


Figure 12: Huddling Chamber Example

Once the disk has begun lifting, there still must be an additional force to keep the disk lifted. This is generated by an aerodynamically designed disk profile that takes advantage of the media flow. Conservation of moment is used as the media flows against the disk's profile which is routed back downwards to produce lifting force. Figure 11 shows this force as the black arrows. This flow force generated by the media passing over the disk profile helps keep the PRV at full lift when the system pressure is sufficient enough to cause the PRV to remain open. Once the system's pressure is low enough that sufficient flow force does not exist, the PRV recloses. However, because of the flow generating force, the PRV will reclose below its set pressure; the point at which it recloses is referred to as blowdown. Blowdown is the difference between the set pressure and the reseating pressure (Hellemans 2009).

The opening movement of a PRV can either being described as static, where the disk opens and remains in the fully opened position during an overpressure relief cycle, or as dynamic, where the position of the disk is a time dependent function. In a static circumstance, media is flowing through a PRV in steady conditions. Ideally a PRV should be described as static, however if the components of a PRV's installation cause flow instabilities during PRV flow, the disk's position will be dynamic. It is in the dynamic cases where a PRV will cycle at high frequency and potentially cause wear to components. Figure 1 shows adhesion wear on a PRV's disk stem and Figure 2 shows wear within the bore of the adjustment screw for example.

Investigations were done to explore the conditions in which unsteady flow and thus high frequency movement of a PRV's disk occurs. There are two terms used to refer to the unstable movement of a PRV's disk which are "chatter" and "flutter." Flutter refers to low frequency cycling while chatter is described as a rapid unstable opening and closing of the PRV's disk (Darby 2013). The American Petroleum Institute (API) defines chatter in API Std. 520 Part I as the opening and closing of a PRV at a very high frequency. Flutter is defined as the abnormal, rapid reciprocating motion of moveable parts. The main difference between these is that chatter happens when the disk moves to the closed and opened position. Flutter is simply oscillatory movement of the disk, not necessarily to a closed position. Chatter and flutter will reduce the relieving capacity of a PRV because the disk is not being held consistently fully opened. A partial opening means that the flow is being reduced because the exit path is not as large when compared against a fully opened disk position. In either case, cyclical movement of the disk's position is predominantly influenced by discharge and inlet piping. Both of these

factors upset the force balanced of the disk and their magnitudes are dependent on the amount of flow entering and leaving the PRV.

There are unintended force components to the force balance of the disk that can affect the total closing force. Pressure that generates in the discharge of the PRV can act on surface areas of the disk and produce force components; this pressure is referred to as backpressure (Cremers, Friedel and Pallaks 2001). The backpressure acts upon all surface areas of the disk. Since there is more area on the top than bottom that the backpressure acts on, it will generate a force that attempts to close the PRV. Figure 13 shows the location of the forces generated by backpressure. The black arrows are the backpressure forces, the blue is the system's pressure force, and the red arrow is the spring force.

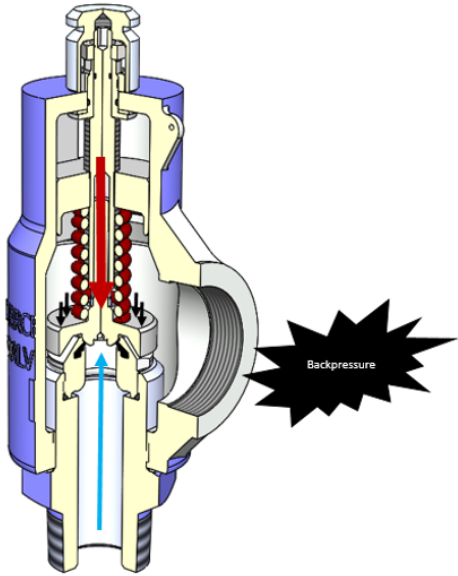


Figure 13: Backpressure Forces on a PRV's Disk

Backpressure comes in two forms which are built-up and superimposed. Superimposed is discharge pressure that exists before the PRV has been opened. Superimposed backpressure was not a focus of this study because it does not induce

high cycle movement of the disk. Built-up backpressure is discharge pressure which has been developed as a result of an opened PRV flowing media through discharge lines. The discharge lines cause frictional flow losses and thus pressure build up within the PRV's discharge space. Built-up backpressure is directly proportional to the amount of mass-flow leaving the PRV and the amount of friction factors within the discharge piping design. Discharge piping grossly affects the amount of built-up backpressure and thus has an influence on PRV disk position stability. Excessive backpressure will increase the probability of chatter (Smith, Burgess and Powers 2011). Figure 14 provides an illustration of a discharge flow restriction that will lead to an increase in backpressure and possible flow instability.

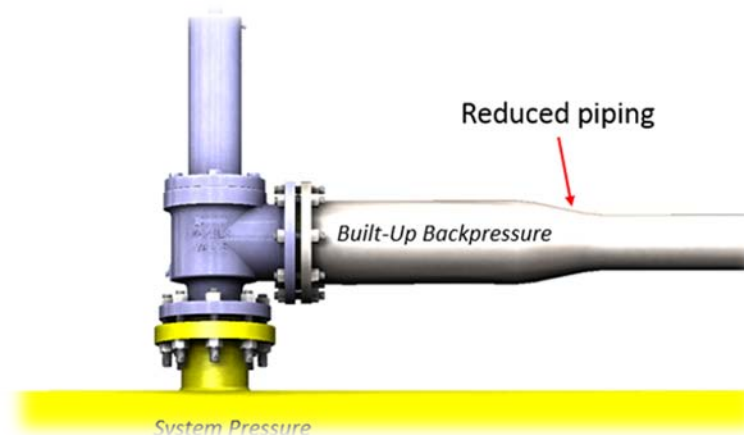


Figure 14: Built-up Backpressure from Discharge Restriction

Inlet pressure loss is a result of a frictional flow loss of media entering into the PRV. Figure 15 illustrates an example of inlet pressure loss existing on a PRV installation. Here, there is a reduction in the inlet piping just before the PRV. This would not affect the static pressure the PRV sees when it is normally closed, however it would cause flow restrictions and thus pressure losses once the PRV is opened. This

affects the force balance on the disk and reduces the force generated by flow, see Figure 11 with this force denoted by P_v and black arrows. It is known that too high inlet pipe pressure loss will cause oscillations as a consequence and the general rule is that 3%, of set pressure, is the allowable limit (API 2013). This however is a conservative rule that does not take into consideration any specific relief valve type or behavior (Cremers, Friedel and Pallaks 2001).

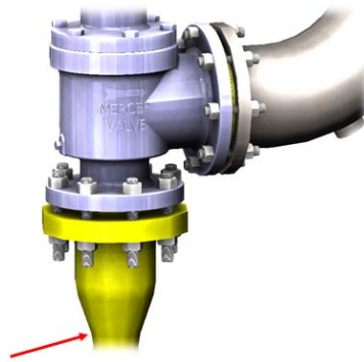


Figure 15: Inlet Pressure Loss Example

The actual cause of chatter and flutter in a PRV is the presence of harmonic disturbances which can cause an instability of media flow and thus upset the force balance within (Bazso and Hos 2013). These harmonic disturbances are the pressure wave fluctuations that occur from flow through the PRV's inlet piping, the PRV itself, and the PRV's discharge piping. The behavior of the disk during an oscillation depends on the spring-mass damping characteristics, the net forces acting on the disk, the blowdown of the PRV, the dynamics of the fluid in the inlet piping including pressure loss and inertial and compressive forces, the fluid dynamics of the discharge line which affect the amount of backpressure, and the disk's lift versus flow characteristics (Darby 2013). The disk behavior during an oscillatory movement is dependent upon the mass of

the moving parts, the spring's stiffness, the dampening of the moving parts, and the total force acting on the disk. The net forces acting on the disk are dependent upon the flow force generated underneath the disk from inertial effects, the spring force, and the instantiations static pressure atop the disk. The blowdown of a PRV is dependent on the net forces acting on the disk and is inherent to the aerodynamic profile of the disk's design. The disk's lift versus flow characteristics are again dependent upon the design of a particular PRV. The inlet piping pressure loss and inertial forces along with the discharge piping pressure increases are dependent upon the piping geometry and the mass flow during a relief event.

All ASME certified PRVs will normally flow in a steady state condition if the inlet pressure loss is 3% or less of the set pressure and the built-up backpressure is 10% or less of the set pressure. It isn't until the installation of the PRV that causes the flow instability, which is generally a result of inlet piping or discharge piping design.

Excessive inlet pressure losses will essentially "choke" of flow generating force which keeps the disk open. If the inlet pressure losses are less than the blowdown pressure, the PRV will operate stability and not oscillate in movement (Smith, Burgess and Powers 2011). If however the frictional pressure losses are too great, then the PRV may not be able to reach the full lift position or oscillate in movement.

Increasing the length of the inlet piping will have the effect of increasing the duration of the time it takes to open the PRV, which increases the amplitude of the oscillations, and lowers the maximum lift ability of the disk (Aldeeb, Darby and Arndt 2014). This is largely due to pressure waves. The amount of inlet piping length will affect the pressure wave leading into the PRV. If conditions exist where the pressure

wave does not travel fast enough from the disk to the pressure source and back prior to the PRV beginning to close, the disk will not be supported by the returning wave (Smith, Burgess and Powers 2011). A combination of the acoustic pressure wave and frictional inlet pressure losses, which are greater than the blowdown, may cause PRV disk instability.

In addition to the inlet piping aspect, harmonics within the PRV system affect PRV stability in other ways. Resonance caused by high velocity fluid has a role in the pressure waves traveling to and from the PRV's inlet. This is caused by vortex shedding (Smith, Burgess and Powers 2011). The other way harmonics have a role is in regards to cavity resonance. This is a phenomenon that occurs when the natural frequency of the piping matches the natural frequency of the PRV's mass-spring system. Cavity resonance will cause pressure wave instabilities.

As explained, the piping system has a large influence on the flow stability of a PRV. When designing the piping system, the flow rate that the pressurized system can produce is normally used. The PRV's orifice is also selected based on the maximum possible flow rate. If however, a selected orifice is far bigger than what is actually required, the PRV will relieve more than what is necessary. The term for when a PRV's orifice is much larger than what is needed for the overpressure application is oversized. An oversized PRV is more prone to instabilities than an appropriately selected size (Smith, Burgess and Powers 2011). The reasoning for this is that there is not enough fluid flowing through the PRV to keep the disk fully opened. The PRV is flowing too much media too quickly. Once the PRV recloses, the pressure builds up since the overpressure event was not fully relieved and the PRV re-opens. Additionally, if the

PRV relieves too much, it may potentially induce inlet pressure loss or outlet pressure build-up because the piping design of the system had not intended for that much flow. In any case, an oversized PRV increases the chance that some form of flow instability will happen.

PRV disk movement in unstable conditions is a time dependent function as a product of the flow. Darby presents a system of equations that includes all factors involved which can be used to model the disk's movement as a function of time. Smith et al. give equations for determining appropriate piping lengths and permissible acoustical frequencies. Cremers et al. elaborate on the "pressure surge criterion" for determining an expected operation state of a PRV in regards to pressure waves. This is all however, not relevant to this work. The main idea found from research on PRV oscillations is that it can readily exist in certain conditions which was shown by Darby in his works.

In relation with PRV's guiding components, the occurrence of galling will undoubtedly result in seizure and malfunction. This is because the presence of worn guiding surface add frictional resistance and may affect the force balance of the PRV. Additionally a severely worn surface may inhibit movement of the disk altogether because of surface interference. Lubrication of the guiding surface would prevent wear of components however most designs do not have the ability to be readily lubricated. Complete removal and disassembly would have to happen to lubricate the wear susceptible parts. Furthermore, the presence of lubricants may attract debris which can interfere and cause resistance to movement and even abrasive effects.

Chapter 3: Methodology

The primary method of data gathering in this work was through research of technical articles that were in the realm of this work's topic. This provided the author with more understanding about the inner workings of friction, wear, metallurgy, flash temperature, and PRVs. However, in order to justify the claim that galling can exist in a low statically loaded sliding contact, physical testing was done on a PRV and a computational fluid dynamics (CFD) problem was conducted. The physical test proved the existence of galling while the CFD analysis illustrated that the static load was low.

The PRV that was examined in this work was a Mercer Valve Co. Inc.[®] model number of 91-17E51T09X1T. This was a conventional spring operated PRV with an "E" orifice designation; the actual area of discharge for an "E" is 0.212 in². The connections were a 1" NPS male pipe thread at the inlet and 1" NPS female pipe at the outlet. A specifications sheet for the associated PRV can be viewed in Appendix A: PRV Specification Sheet.

CFD Simulation

The CFD analysis consisted of examining a solid computer-aided-design (CAD) model and inputting it into a flow simulation software. The program used for the CAD modeling was SolidWorks[®] and the CFD simulation used a SolidWorks[®] add-on entitled Flow Simulation. The CAD model reflected, as far as flow geometries, the physical PRV that was tested. The goal of the CFD simulation was to determine the drag on the disk since that represents the normal load applied on the surfaces of the guiding components. The drag force "pulls" the disk towards the outlet of the PRV but other guiding components keep the disk in place and aligned axially. This was done at

various disk lift positions to determine the overall normal load on the components subject to galling. United States Customary (USC) units were used in the study.

In the simulation, air was used at standard conditions as the media because it imitated the media used in the physical testing. The computational domain was reduced to only include the internal volume of the PRV because it was the area of interest and a larger domain would only increase the time duration of the simulation. The domain space is shown in Figure 16.

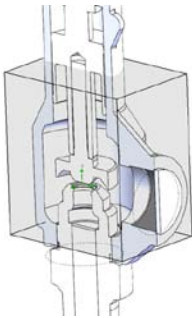


Figure 16: CFD Computational Domain

The mesh used in the simulation was a global mesh setting with an initial detail level of four out of six. The total number of cells was 53484 with 19793 fluid cells contacting solid surfaces. A section of the mesh is shown in Figure 17.

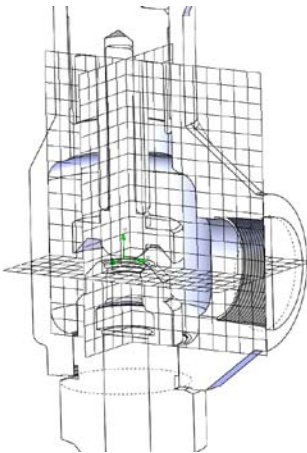


Figure 17: CFD Mesh

Goals, also known as sensors, were used to get the necessary parameters. A "lift force" parameter was placed on the bottom surfaces of the disk. The purpose of this was to determine how much force was being generated by the flow. A "side force" goal was used on all surfaces of the disk to determine the drag component that occurs during flow. A "down force" parameter was placed on the top surfaces of the disk. Its purpose was to observe the force acting downwards on the disk. An "average static pressure" goal was placed on the top and bottom surfaces of the disk. The purpose of these two goals was to observe the pressure balance on the disk.

The inlet and outlet of the PRV's CAD model were defined and given initial conditions. Initial boundary conditions were applied to the model which is shown in Figure 18. At the inlet location, a pressure of 124.7 psia [860 kPaa] was defined. This was determined by using the flowing pressure of a PRV set at 100 psig [689 kPag]. This was the set pressure plus the allowable overpressure in absolute units. This would be the theoretical pressure the PRV would keep the system from exceeding. A mass flow rate of 0.505 lb/sec [0.229 kg/sec], was placed on the outlet of the PRV. This value was determined by equations presented by ASME for determining flow through a PRV in a gas critical flow application. This calculation can be viewed in Appendix A: PRV Specification Sheet.

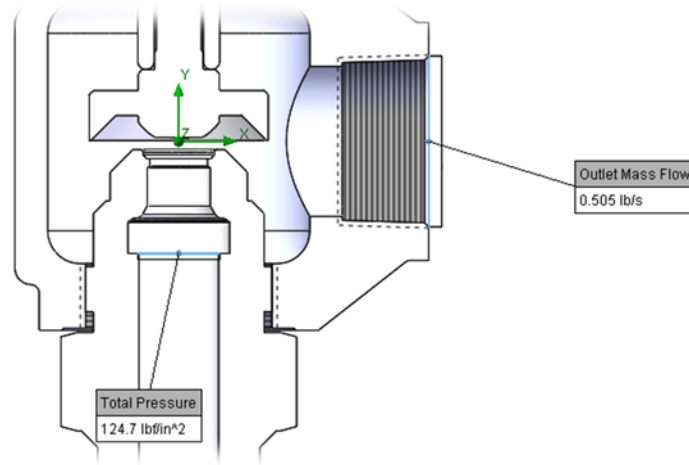


Figure 18: Initial Conditions of CFD Simulation

The method of CFD simulation used to determine the drag component on the disk was appropriate because the disk has a non-conventional geometry and would have been difficult to determine otherwise. It has been used for the analysis of PRVs in other studies (Song, et al. 2014). The boundary conditions and set-up for this simulation assume steady-state flow with a defined mass flow through the exit. This is mostly reflective of a typical PRV relief event in stable, non-oscillatory, conditions. It would be the case for determining the greatest value of drag on the disk because its amount is mostly dependent upon the amount of flow. In this case, the maximum achievable mass flow was used for this particular orifice sized PRV.

The method of utilizing CFD was analyzed simply by receiving the solution outputs given by the goals of the model. The values were examined carefully to determine if they made physical sense or if they were erroneous. The drag forces seemed legitimate however the lift force and down force goals seemed a little off when different disk positions were used. This is probably because the boundary conditions were not changed though different disk positions were. At different disk positions, the

inlet and outlet parameters are likely to dynamically change. Furthermore, this model did not consider any dynamic flow conditions and may have been over-simplified. This was a moot point since the ultimate goals of the analysis was to determine the static load of the components.

Physical Testing

Physical testing was an important part of this study because it showed a real life example of the conditions that this work focused on. Testing was done by installing a PRV onto a pressurized system in such a way that flow instability would be readily induced. Flow instability was produced by two means, restricting the inlet and restricting the outlet. Figure 19 provides a depiction of the testing arrangement used. The goal of this test was to observe the wear susceptible components before and after an instable relief flow event. This showed that under certain conditions, the components involved would begin to show signs of severe adhesion wear. The primary components in question were the guiding portion of the disk stem and the guiding bore of the adjustment screw.

A 1 inch full-port ball valve was used immediately prior to the inlet of the PRV, to control inlet flow restriction. Approximately 2 feet of 1 inch schedule 40 pipe was placed on the outlet. Additionally, a 3/4 inch reduced-port ball valve was used on the end of the 1 inch discharge piping which enabled control of the discharge flow restriction. The final exit of the discharge was to atmospheric conditions. The system the PRV was installed upon had a generous supply of media. It was approximated as an infinite supply of flow because it had several large vessels which had a volume of over 700 cubic feet at a pressure in excess of 3000 psi. This was more than enough media

and presented no limitations. The vessel the PRV was installed on had a volume of 35 cubic feet. This was enough volume to get the PRV to achieve full lift and flow at steady state conditions. The pressure of the vessel was readily controlled by a gate valve which was located between the supply volume and the test vessel. This gave the ability to control the pressure of the vessel and the rate at which it was pressurized.

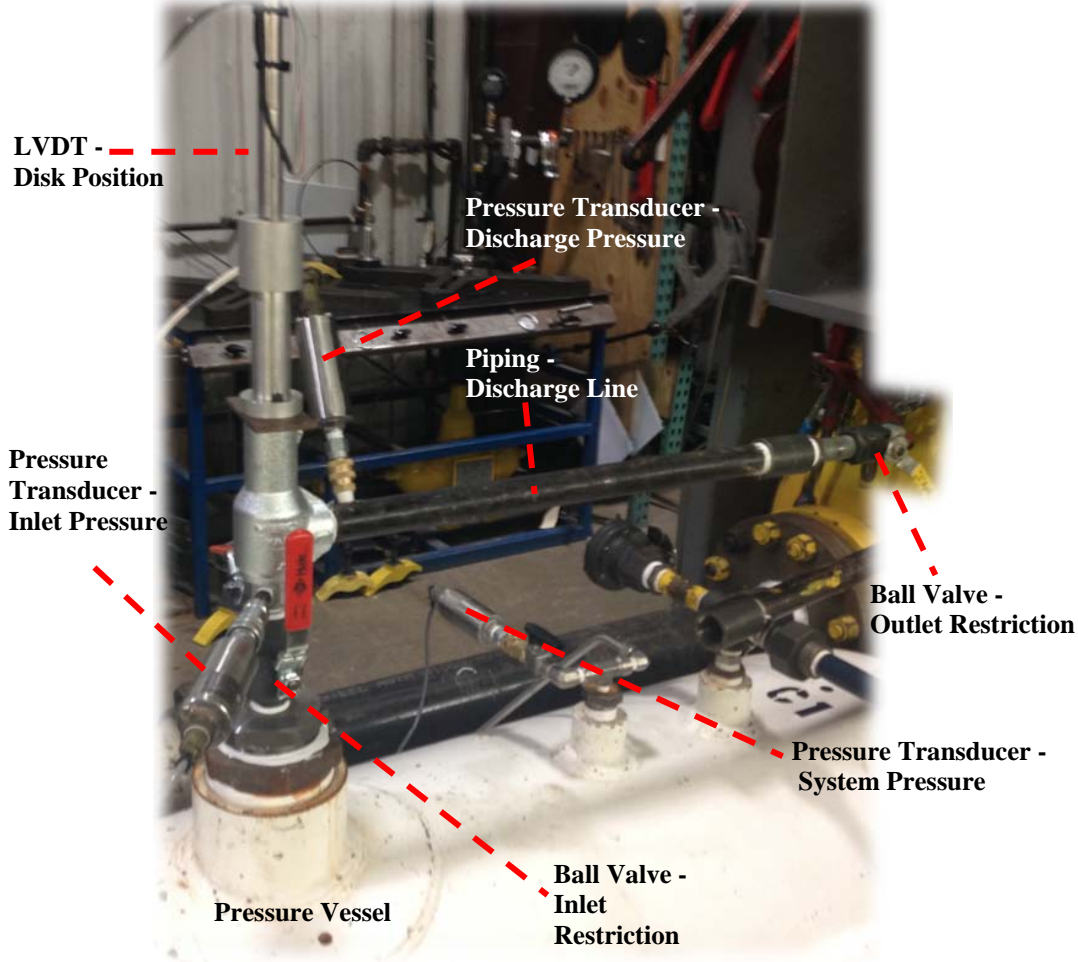


Figure 19: Test Set-Up

The testing system was instrumented with sensors to monitor and record data. A pressure transducer was used atop the vessel to monitor the overall system pressure. A pressure transducer was located immediately prior to the PRV's orifice; it was located

between the inlet restriction and the disk. This provided the means to monitor the pressure that the PRV's disk was actually being exposed to. A pressure transducer was located immediately after the PRV's outlet to monitor the discharge pressure directly after the disk. All pressure transducers used were Honeywell Sensotec Sensors, model TJE, part number 060-4255-11TJG. These had a scale of 0 to 750 psi. It is important to note that the pressure transducer are only able to measure instantaneous static pressure, not pressures generated by flow velocities. Pitot tubes would have provided more accurate pressure monitoring as they are able to capture transient pressure that is a product of flow velocity. This type of sensor was not available at the time of testing. The pressure sensors provided data that would be used to observe pressure disturbances when a flow restriction was imposed.

A linear variable differential transformer (LVDT) was used to monitor the position of the disk. Special appropriations were made to accommodate an attachment of the LVDT sensor which is shown in Figure 20. The top of the disk was drilled and threaded so that a rod attached to the LVDT may be equipped. The LVDT used was a Macro Sensors, model DC 750 1000. From the data outputted by the LVDT, the disk's speed and oscillation frequency was able to be determined.



Figure 20: Disk Stem with LVDT Attachment

All measurement instruments used were tied into a data acquisition system. The system used was a DaqBook/2000 with a DBK65 module. This provided the ability to record data and output all the data points for each sensor for analysis into Microsoft[®] Excel[®]. The sampling rate used was 80Hz. The data acquisition system was able to have a larger sampling frequency, however this was about that the LVDT was able to output data. The limit was determined by initial trial and error. It was found that increasing the sample rate only presented diminishing returns as far as data quality and the amount of data noise only increased. The data acquisition system consisted of various modules that enable sensor hook up and gave the ability to output a digital display. This is shown in Figure 21.



Figure 21: Data Acquisition System

An experimental PRV was provided by Mercer Valve Co. Inc.[®] for testing of this work. The tested PRV's specification sheet can be seen in the appendix for reference. The components used within the PRV were of 316/316L stainless steel and their associated material certifications can be viewed in Appendix C: Component Material Certification. The PRV was tested with set pressures of 100 psig [689 kPag]

and 300 psig [2068 kPag]. Multiple disk stems and adjustment screws were used to examine different severities of oscillatory movements of the disk. Initial pictures of the parts were taken to baseline what they should normally look like.

The testing process began by calibrating the set pressure of the PRV. This was done on a test-stand that allowed the user to accurately control inlet pressure and adjust the compression on the set spring so that the PRV will open as intended. Once this was done, the PRV was installed on the test vessel. With the inlet and outlet ball valves completely opened, hence limited pressure loss or build-up, the vessel pressure was brought to the point where the PRV should open. This was done to ensure functionality of the PRV and establish a baseline of normal operation. Once this was done, flow restrictions were applied by actuation and modulation of either ball valve located at the inlet and outlet. Several different severities of flow oscillations were done which after each test run, parts were examined and data was collected. This was conducted by gradually increasing the severity of flow instability until galling wear was observed on the PRV's components.

Data was analyzed in this work by graphical plotting of various outputs against time. This provided a good visual representation of the cycling that occurred for each of the measured variables. The frequency of the movement was able to be measured by a simple cycle count when the position of the disk was measured against time. Pressure fluctuations were able to be observed and could be overlaid against the disk's position which provided some correlative evidence of how pressure is related to the instability of the disk's position. Finally, before and after images were used to determine a comparison between wear for different severities of oscillations. This was the ultimate

goal of the experiment and images provided the necessary depiction of the claims of this work.

This method of testing had a few drawbacks but it is justified for the overall goal of this work. The flow of the PRV was able to be controlled and as a result instability was induced. The disk's movement was able to be cyclically loaded so that wear would occur. The cyclical movement resembled like PRV applications in which a restriction of flow would occur. A similar method of testing flow stability was done by Aldeeb et al. in which inlet and outlet piping was examined and a PRV was physically tested. The sampling rate used in that accomplishment was three times greater than this work. Examining that aspect, the sampling rate used in this method may yield results of the disk's position that may possess a greater value of error. Furthermore, the usage of pitot tubes may have provided a better means to record the transient pressure waves generated by the flow restrictions. Finally, the utilization of pictures was adequate in the documentation of the existence of galling wear on the components however it has limited usages. An electron beam microscope would have provided more details and would have been better at determining the onset of galling. One could have seen the beginning stages of adhesion wear and referenced it against the number of cycles the parts went through. Nevertheless, the usage of macro level images furnished the required information for identifying galling.

Chapter 4: Findings

Information was gathered in this work to help validate its postulate. The CFD simulation results were examined, existing conventional equations were applied, and physical testing was done during this work.

CFD Simulation Results

It was found by a CFD simulation of a PRV that the drag component, side-loading, of the disk subassembly did indeed have a relatively low value. Various disk positions ranging from almost completely closed to fully opened were examined to determine the maximum value, which was found to be around 1 lbf [4.45 N] of side load. This supported the notion that there is very little side loading on a PRV's disk subassembly.

At the full lift position, there is a substantial amount of force generated by the media flowing underneath the disk in the direction that holds the disk open. Shown in Figure 22 is the pressure profile and flow trajectories profile plot. Here it can be seen that the flow lines change directions just under the PRV's disk which generates force from a change in momentum direction.

It can also be seen in Figure 23 that there is a portion of the underside of the disk which is exposed to a greater pressure than the upper side. This generates an additional force component in the opening direction. Figure 24 shows the influence that the huddling chamber geometry has on the lift generating force component. The greater angle the "wings" of the disk have, the greater force is generated as a result of static pressure being captured and an increase in flow momentum direction change. This huddling chamber design has an effect on disk position stability as well. If the primary

lifting force component is the flow forces, upsets to the flow velocity will undoubtedly affect the position behavior of the disk. These figures help illustrate what was explained in Chapter 2: Theory and Literature Review in regards to the upsets in force balance causes in disk position instability.

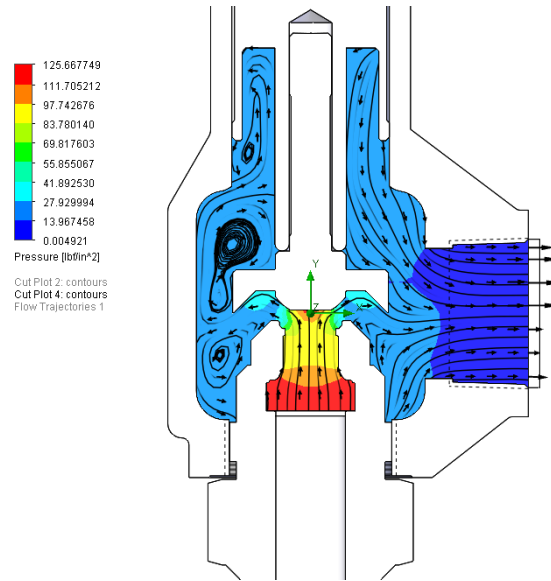


Figure 22: Full Open Pressure and Flow Trajectories Profile Plot

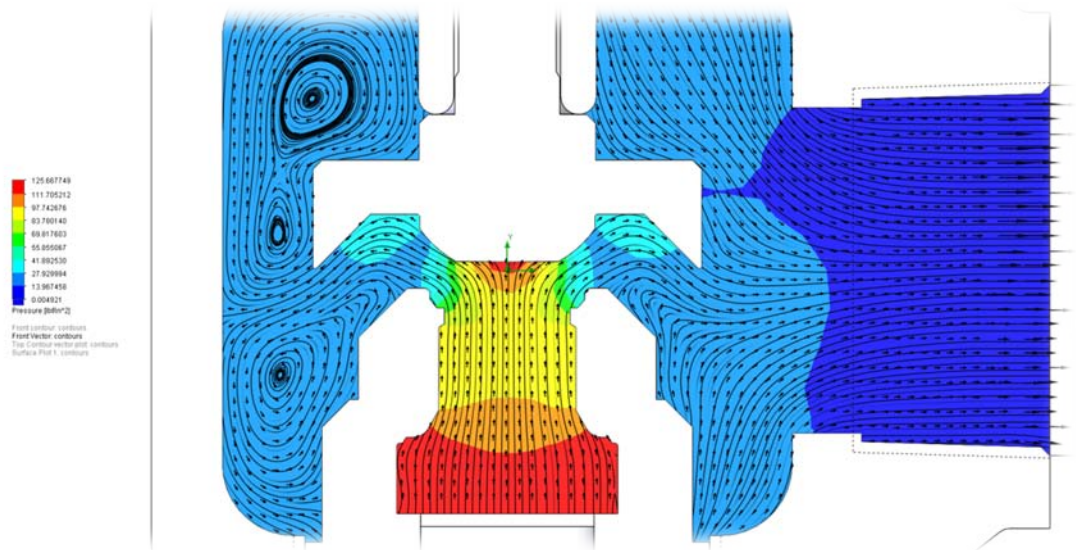


Figure 23: Detailed View of Flow and Pressure Profiles

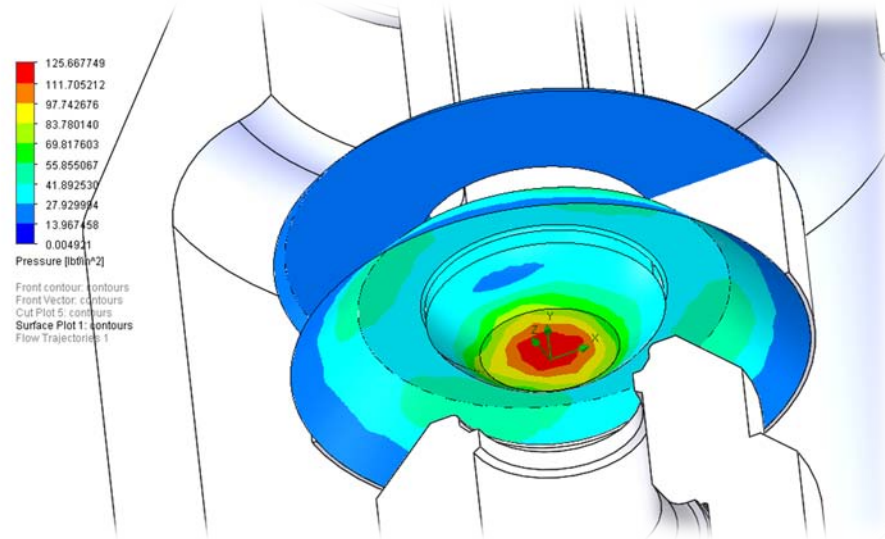


Figure 24: Pressure Profile of Disk

Various disk positions were examined to determine the maximum value of the drag force on the disk and also to observe any trends. The results are found in Table 3. It was found that as lift increased, the amount of side loading also increased. The correlation made practical sense because as more media is flowing, its density and velocity would also increase; density and velocity have a large bearing on the drag force equation. The drag force was found to be low in comparison to the other forces involved. The drag force was found to be in the direction of the x-axis which was aligned with the outlet of the PRV. This was expected since the flow "pulls" the disk towards the exit.

It was found that as lift increased, the force generated to lift the disk also increased. This also made practical sense because as more media flows over the disk, more momentum change occurs. The purpose of this finding was to observe the force that the PRV undergoes to open.

Table 3: CFD Simulation Results

Lift	Lift Force		Drag Force	
	<i>lbf</i>	<i>N</i>	<i>lbf</i>	<i>N</i>
100%	42.0	186.8	1.1	4.9
75%	38.9	173.0	1.1	4.9
50%	32.4	144.1	0.9	4.0
25%	21.7	96.5	0.6	2.7
5%	14.0	62.3	0.3	1.3

Additional CFD results are provided in Appendix B: Additional CFD Study Results for further review of convergences and values for the interested parameters.

Physical Testing

The results of the physical testing showed that galling occurred when high cyclical movement of the disk occurred. Several test runs were done with various conditions that induce different levels of oscillations. The level of severity was increased to the point where galling of the suspected components occurred. Three sets of components were examined, labeled as I, II, and III sets. Before testing began, surface roughness was measured in an effort to omit the notion that initial surface finish caused the galling. The surfaces of the components were smooth prior to the test runs. These measurements are shown in Table 4. Prior to testing, pictures were taken of the surface conditions which is shown in Figure 25.

Table 4: Surface Finish

ID	Adjustment Screw Bore	Disk Stem
I	68.2	16.1
II	51.5	27.5
III	41.5	12.7
units in $\mu\text{in rms}$		



Figure 25: Initial Surface Condition of Disk

The first test run used components I and a low amount of flow instability was induced once the PRV opened and was flowing. It was found that in a low severity of disk instability, the disk moved with a velocity of 11.8 to 14.0 in/sec [0.3 to 0.36 m/s] at a frequency of 40 to 45 Hz. This was found by analyzing the recorded data of the first test run. This can be seen in Figure 26 where disk position is plotted against time. A section of the oscillations from time 0.9 to 1.15 seconds was taken to count the number of oscillations to determine a velocity and frequency. This can be seen in Figure 27. There, it was observed that the disks movement traveled between a displacement of 0.1 to 0.25 inches. This means that the disk moved up and down but did not reach full lift or fully closed while undergoing the oscillations; full lift would be equal to a displacement of 0.31 inches.

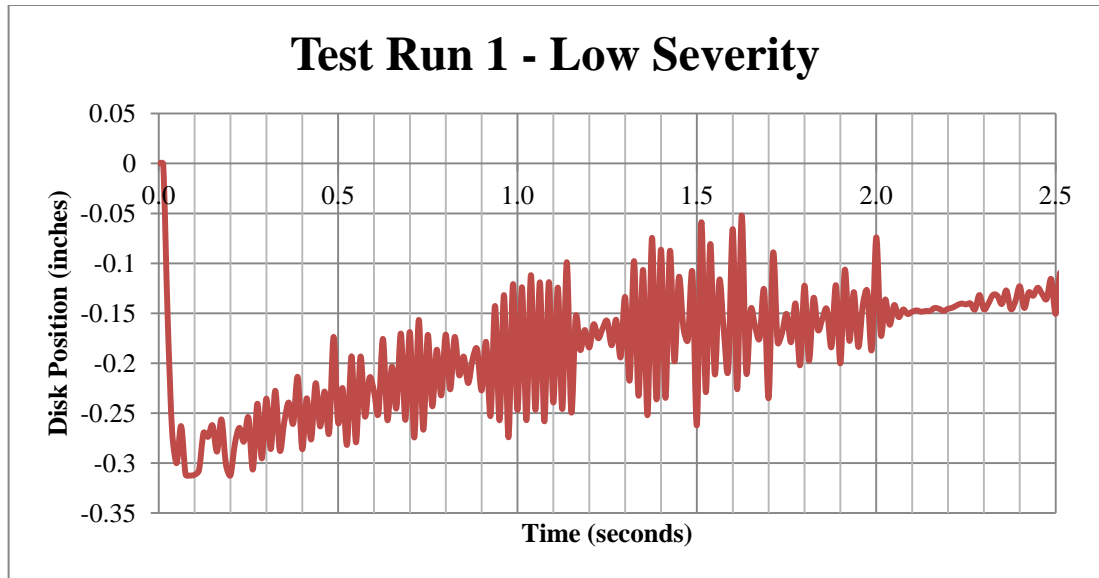


Figure 26: Low Severity Test Run

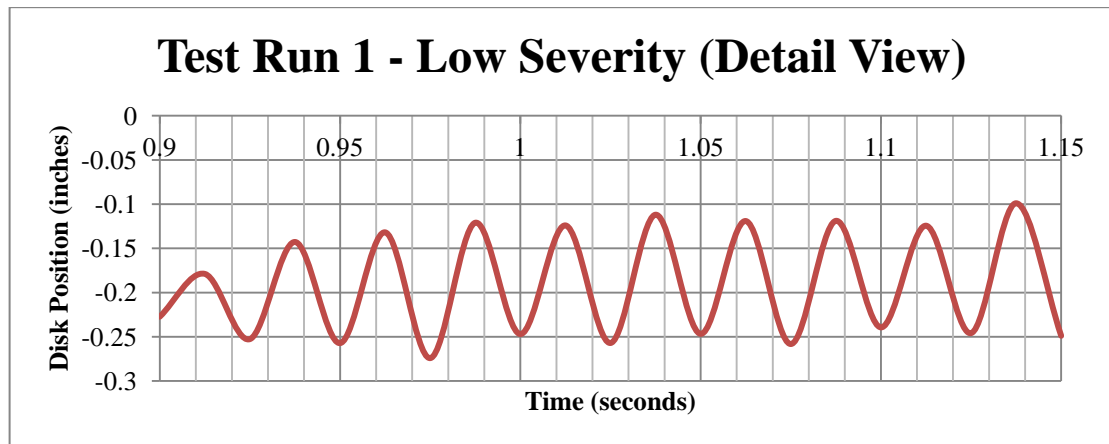


Figure 27: Low Severity Test Run Detailed View

The disk was inspected and found to show signs of wear but not to an extreme adhesion wear level. This is shown in Figure 28. One was able to observe polishing of the disk at the points of rubbing contact but no signs of adhesion wear.



Figure 28: Low Severity Wear on Disk

Component set II was installed and used in a medium severity test run. Flow instability was induced by restricting the inlet and outlet more than the low severity test run. It was found that in a medium severity test run of disk instability, the disk moved with a velocity of 11.0 to 14.0 in/sec [0.28 to 0.35 m/s] at a frequency of 30 to 35 Hz. This was found by analyzing the recorded data by plotting disk position over time which is shown in Figure 29. A section of the oscillations from time 0.2 to 0.4 seconds was taken to count the number of oscillations to determine a velocity and frequency and can be seen in Figure 30. There it was observed that the disks movement traveled between a displacement of 0.07 to 0.23 inches. This means that the disk moved up and down but did not reach full lift or fully closed while undergoing the oscillations.

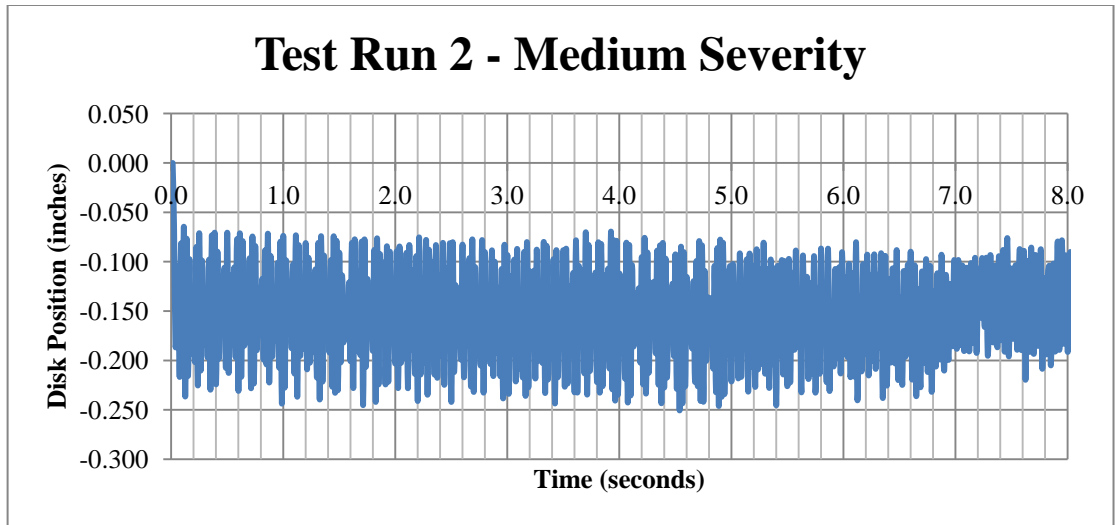


Figure 29: Medium Severity Test Run

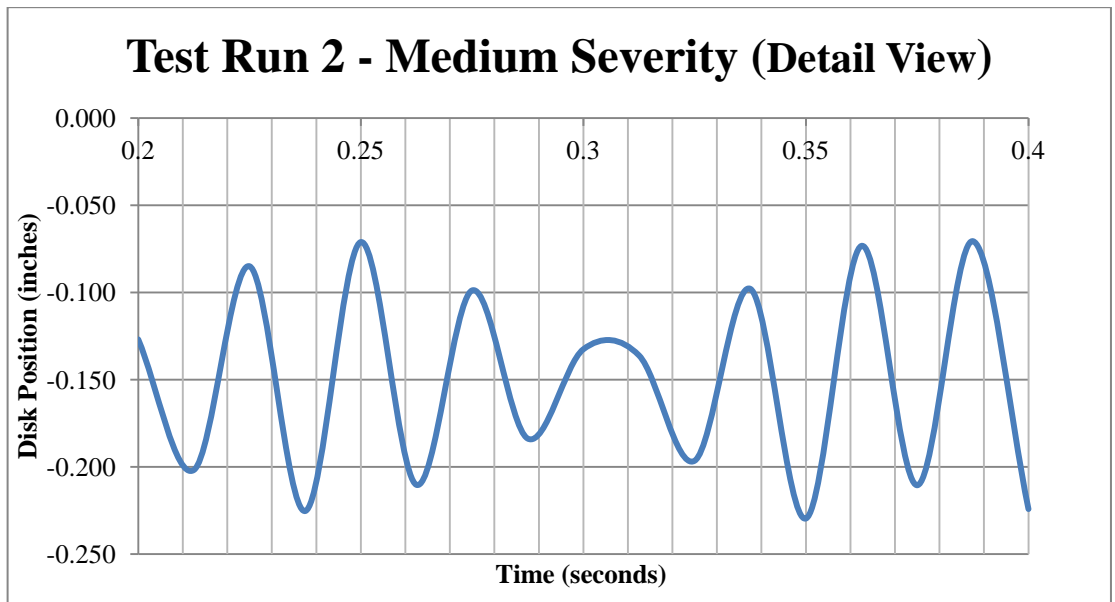


Figure 30: Medium Severity Test Run Detail View

The disk was found to have signs of wear similar to the previous test run which is expected since both runs had about the same disk velocity and frequency. This is shown in Figure 31. The disk showed signs of polishing at the rubbing contact points.

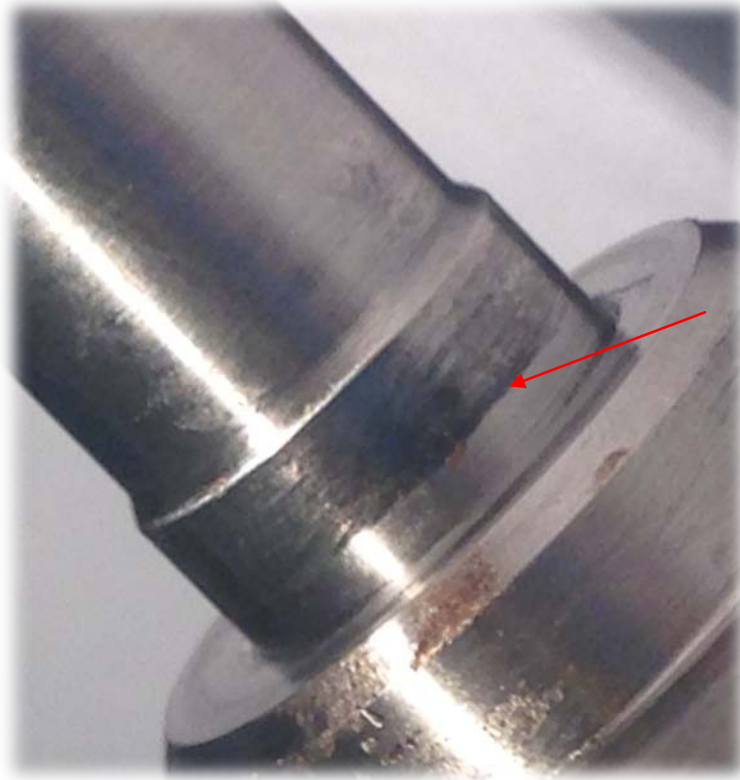


Figure 31: Medium Severity Wear on Disk

In the final test run, the set pressure of the PRV was increased from 100 to 300 psig [689 to 2068 kPag] to increase the disk's closing force magnitude. It was determined that the set spring was not applying enough closing force to cause the disk to reach fully open and fully closed during a flow instability event. The disk was simply fluttering between full open and closed position without reaching the ends of the travel limits. A stiffer spring associated with a greater set pressure would cause a more severe movement of the disk.

During the high severity test run, the speed of the disk was found to be 17.7 to 35.3 in/sec [0.45 to 0.9 m/s] with a frequency of 25 to 30 Hz. This again was found by examining recorded data and plotting disk position over time. This is shown in Figure

32. A detailed sample was used to count the number of oscillations from 0.2 to 1.0 seconds which is shown in Figure 33. It was observed that the disk's position varied between 0.22 to 0.0 inches which means that the disk wasn't quite reaching full lift but was completely reaching the fully closed position.

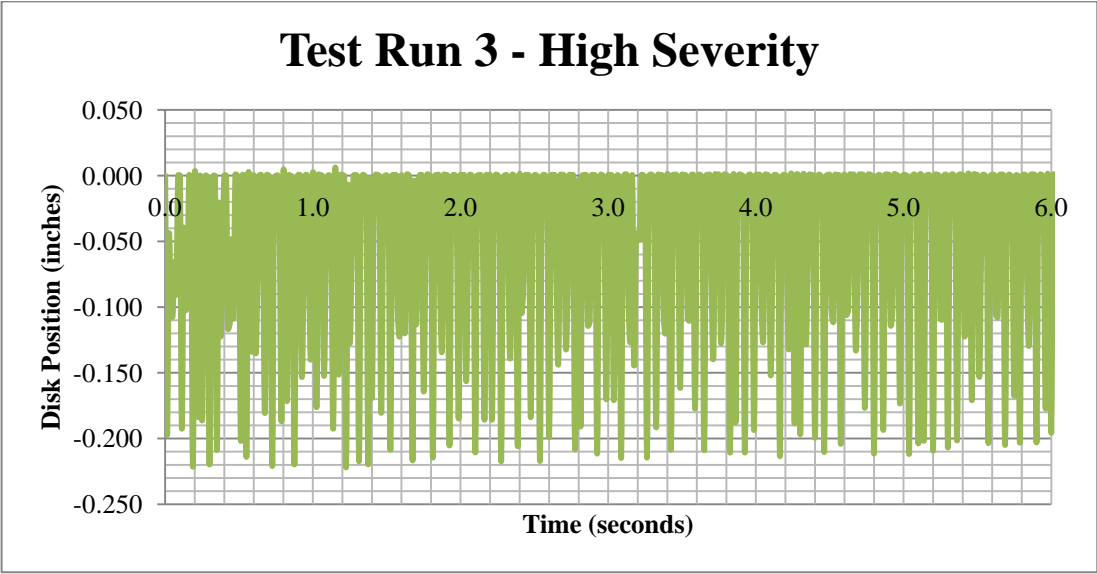


Figure 32: High Severity Test Run

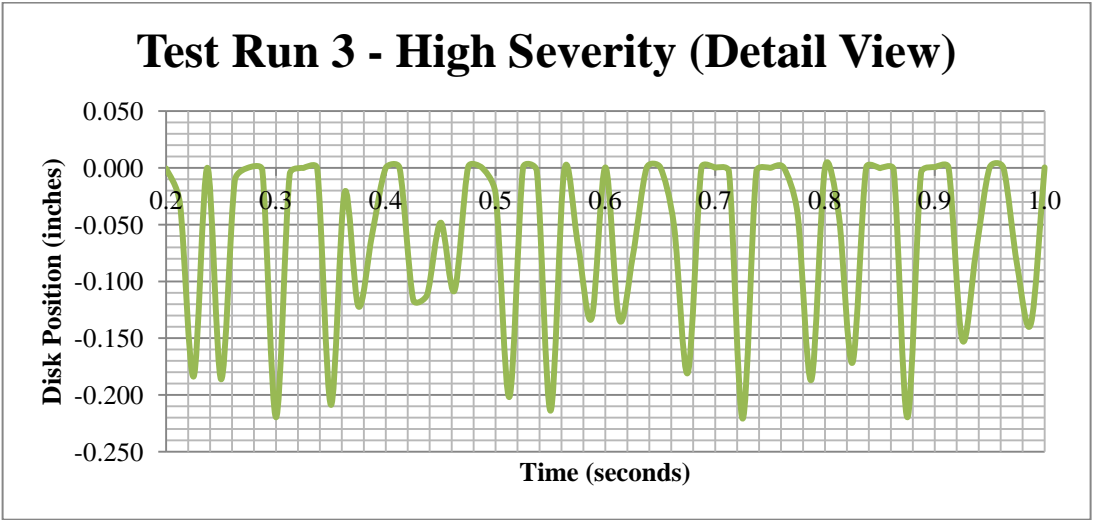


Figure 33: High Severity Test Run Detail View

The disk, as well as the adjustment screw, was found to have signs of galling wear which can be seen in Figure 34 and Figure 35 after this test run. The area of wear was characteristic of severe adhesion wear by its shiny and axial grain appearances. It was highly localized at the area where the disk rubbed against the adjustment screw bore. This was as expected since the velocity of the disk was greater than the two previous test runs.

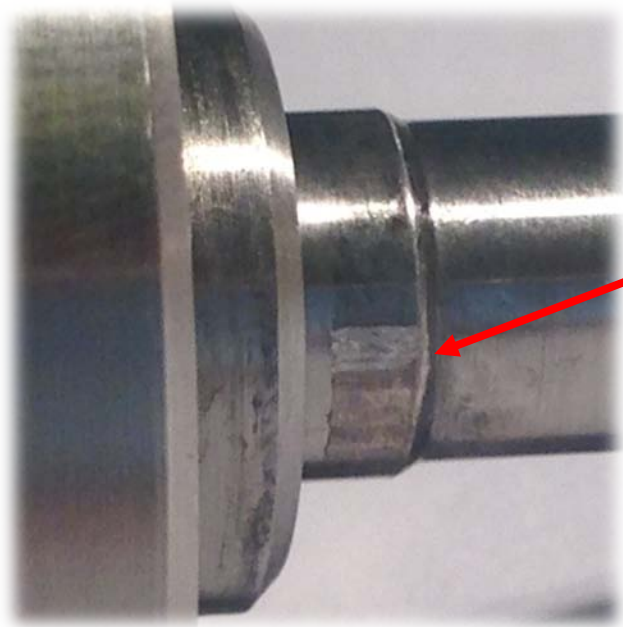


Figure 34: High Severity Wear on Disk

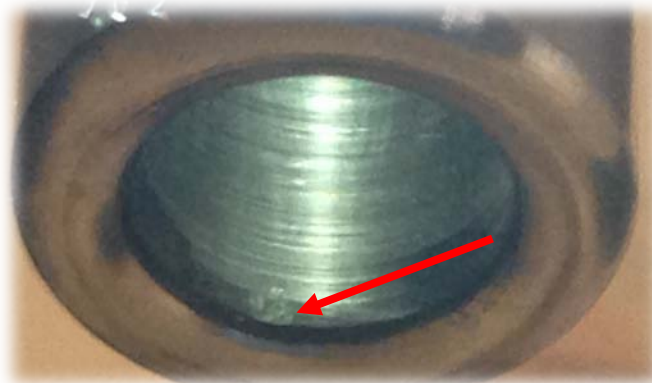


Figure 35: High Severity Wear on Adjustment Screw

In all the test runs, pressure in the inlet and outlet was monitored to help verify that disk stability is a function of a pressure difference acting on the disk. This can be seen in Figure 36. As the pressure difference oscillates, the disk's position oscillates as well.

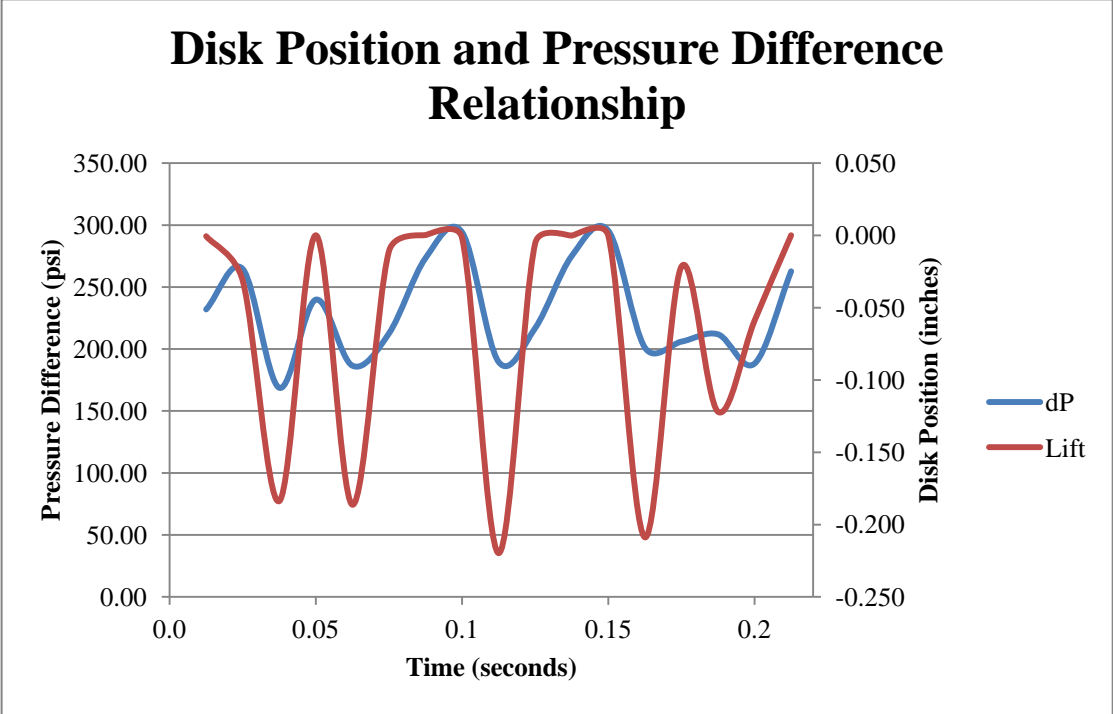


Figure 36: Disk Position and Pressure Difference Relationship

Conventional Model

Theoretical equations presented in Chapter 2 were applied to verify that this work's specific application is atypical to the convention of galling and adhesion wear. Equation 1 and Equation 2 listed that one may determine the amount of material removed during an adhesion wear event by relating the surface hardness and normal load. From the CFD simulation it was determined that the normal load was equal to about 1lbf. The sliding distance was measured to be approximately 0.22 inch. The hardness was found from ASM standards for 316 stainless steel to be BHN 150 which is

equivalent to 73 ksi. A wear factor of 2×10^{-5} was looked up for typical stainless steels in rubbing contact, it was not specific to 316 type (Hamrock, Schmid and Jacobson 2005). According to Archard and Rowntree, usage of the maximum value of the friction coefficient may be used in the temperature calculation of rubbing bodies so this is an acceptable approach (Archard and Rowntree, Metallurgical Phase Transformations in the Rubbing of Steels 1988). It was predicted that the amount of wear volume should equal about 2×10^{-11} cubic inches, which is very small. This showed that this method seems inaccurate since the normal load is so small yet had a large bearing as far as a variable.

The frictional force for the sliding contact of the PRV was determined by Equation 7 in which a coefficient of friction equal to 0.5 was used which was associated with stainless steel rubbing against a harder mild steel; this look-up value was not specific to a 316 stainless steel rubbing against another 316 stainless steel so in actuality the value may be different (Hamrock, Schmid and Jacobson 2005). It was found that the frictional force would be about 0.5 lbf which is very low due to the lack of normal loading. This showed that the shear strain on the surface existed but was not tremendously large.

The maximum attainable flash temperatures were examined based on the recorded velocities of the testing and the normal loading determined through CFD simulation. Using the figures and equations presented in the Flash Temperature Concept section of Chapter 2 and by Jaeger, it was found that the maximum attainable flash temperature was 220 to 440 F [104 to 227 C]. Several assumptions had to be made to determine this. It was assumed that the material properties remained constant including

the specific heat capacity and thermal conductivity. The area of contact was approximated as being very small which is in accord with frictional contact theory in which the true area of contact is much smaller than the apparent area.

Markov's criteria listed in Table 1 was used to help classify the mode of wear that was occurring within the PRV's guiding components. Markov attested that there are two energy types of adhesion wear. Since the measured velocity in the third test run was greater than 0.4 m/s [15.7 in/sec], it can be classified as being a high energy type which would mean that the wear occurring is either scuffing or galling. The two previous test runs did not exhibit speeds greater than 0.4 m/s [15.7 in/sec] which means that they were of the low energy type. It was predicted that the surface temperature of the contacting components would reach up to 436 F [224 C] though the flash temperatures. These theoretical temperatures are much lower than the crystallization temperature; 316 stainless steel which would normally have a melting/crystallization temperature above 2500 F [1370 C]. Applying Markov's criteria for the subtypes of adhesion wear, since the surface temperature was not greater than the crystallization temperature, it falls into the galling category of adhesion wear.

The direction of material transfer depends on which surface has a greater adhesion energy according to Equation 8. The surface with a lesser surface energy will receive the transferred fragments. Since both of the surfaces were of 316 stainless steel and had equal surface energies, the direction of transfer could not be readily determined by Equation 9. It was found through the physical testing that material transfer occurred upon both surfaces. This is somewhat expected since neither side was more favorable.

Chapter 5: Discussion

What makes the case study in this work unique is the fact that severe adhesion wear is evident in a sliding interaction between two lightly loaded surfaces. The classical method for determining galling wear did not have a direct application for the conditions of this work's study because the normal loading was lacking. In typical adhesion wear, material transfer is caused from continuous plastic deformation, adhesion, or a combination of the two as a result of applied loads on the rubbing surfaces (Karlsson 2012). In this case study, continuous plastic deformation did not exist because the normal loads were small. Furthermore, the rate at which these surfaces slide is fast and oscillatory in manner. It is because of the speed, the oscillations, and the material composition that galling exists in this specific situation.

In adhesion wear, the severity and type are dependent upon several things which include friction, temperatures, material properties, and the material's surface properties. Surfaces interact and collide during a sliding event which causes this form of wear. Metal surfaces are never perfectly smooth and possess surface high-points called asperities. This is due to the natural randomness of crystal formation, surfaces defects, and other random natures. The asperities of both surfaces contact each other and the weaker of the two will shear off and separate as small fragments. Adhesion wear would not exist if breakages did not occur. This is possible if both asperities simply deflect since their allowable shear stress was not exceeded. For this reason, harder metals do not exhibit galling as readily as softer metals. Once a fragmentation happens, energy is released and the fragment adheres to one of the sliding surfaces again. The fragment can re-crystallize and weld to the surface due to the generation of heat or it may adhere

because of the forces that caused plastic deformation which smeared it against the surface. Whether the fragment sticks is characteristic of its strength and its strength/temperature relationship. Adhesion of surface asperity junctions occur easily when the surfaces are very clean and will create metallic bonds (Bowden and Rowe, The Adhesion of Clean Metals 1956). There is a natural tendency for like materials to bond together. The adhesion comes from strong metallic junction bonds and will be proportional to the amount of normal load first induced between them. In this work's specific case, the sliding materials were of the same composition which increased the propensity for galling to occur.

The initiating component to, though not the entire dependence of, the existence of galling in this situation begins with the generation of friction forces. Friction between the surfaces must exist for any type of wear, whether it be from abrasive or adhesive effects, to occur. The theory of friction denotes that the force generated by friction is equal to the normal load times the coefficient of friction between two surfaces. Additionally, plastic deformation of the surface asperities existed even under small loads due to the true area of contact being so small and yet supporting the applied load. Given this fact, a normal load must exist since it is evident that wear occurs in the case study of PRVs. The material used in the study for both sliding surfaces were 316 stainless steel in the annealed conditions. The components were machined from round bar using a turning process. A turning process, even on a mass production quantity level, produces relatively good surface finishes. The surface finish has a tremendous effect on the coefficient of friction and thus the frictional force component as well. The surface finish of the parts was approximately 54 and 19 μin RMS between the bore of

the adjustment screw and outer diameter of the disk respectively. For a sliding fit, these surface finishes are adequate and would not be a culprit of high frictional forces.

During the friction process, surface asperities are broken off from their original substrate. Wear in a sliding interaction will always present itself as some form of dissipated energy (Jahangiri, et al. 2012). The energy comes from the breaking of the asperity's junction bond. When adhesion wear occurs, the coefficient of friction increases since the surface is roughened. There is a general relationship between surface finish and adhesion wear. As a surface increases in roughness, there is a greater tendency for metal to be transferred to a surface, particularly if the harder material is rough (Hanson, et al. 2007). As shown by Equation 4, the surface roughness will directly result in a greater friction force and thus heat generation. An increase in the friction force will increase shear stress and induce more plastic deformation along the surface layers. Never-the-less, a better surface finish will not grossly affect the incident of adhesion wear, it may simply prolong the time at which it occurs.

The characteristics of breakages in asperities and thus the occurrence of adhesion wear is highly dependent on the metallurgical aspect of the surface material. The sticking of the asperities is additionally dependent on the metallurgy of the materials. 316 stainless steel is known to have a relatively high stacking fault energy which is related to how easily the unit cells of the crystal lattice can be dislocated. Austenitic stainless steels have a face-centered-cubic lattice structure which is easily dislocated. Furthermore, it has a substantial amount of nickel content which has a high stacking fault energy, about 450 mJ/m^2 . (LeMay 1981). This enables the ease of cross-slip and thus breakages of surfaces when frictional forces occur. The material's surface

energy has an association with the sticking of fragments. The direction of metal transfer occurs from the component with smaller surface energy (Chen Adhesion Theories). Surface energy is the molecular attraction forces of the metal; this is how well the materials stick. This influences not only the direction but also whether the fragments actually stick to the surface or remain as loose particles. Austenitic stainless steels have high surface energy which tend to stick to itself. These metal types have a reputation for galling in other applications. Furthermore, fragment transfer is dependent on interface separation and junction adhesion, which is all related to the surface energy.

All of the material transfer during galling must occur at the surfaces of the rubbing bodies. The threshold of severe adhesion wear is only subject to frictional heating and mechanical properties of the surface layer (Markov and Kelly 1999). It was important to examine that aspect since austenitic stainless steels normally have an oxide layer which includes the asperities. The ductility of an asperity has an influence on the adhesion effects. It was suspected that work hardening did not occur due to the low amount of strain energies involved in this type of application; this is because there was a very low static load applied.

The oxide surface layer on a stainless steel has a large role in the interactions of sliding wear. The oxide-absorbed surface will influence to a great extent the rate and type of wear (Markov and Kelly 1999). The oxide layer will initially help prevent adhesion wear until they are removed. If surfaces are subject to poor fracture wear performance, the hard material will damage the opposing surface and a continued plastic deformation process will occur; this all results in increased galling (Hsu, Ahn and Rigney 1980). What may be occurring is that the hard oxide surfaces rub and one

side eventually breaks off in a normal brittle wear fashion. Once the surface layer is removed, the soft bulk material is exposed and adhesion wear begins. The surface of the metal is removed during sliding which exposes a soft and weak bulk material. As the oxide layers are stripped, material transfer occurs but the oxide layer can renew itself when the contacts are interrupted. However, the oxide layer that exists in stainless steel is very sticky (Hanson, et al. 2007). Metal to metal contact of the substrate is not required for material transfer to occur directly since the oxide surface layer may be transferred. The shearing of the oxide layer adds to the plowing factor of friction. The interruption duration for the re-growth of oxide layers is inversely related to the sliding speeds; as the speed is increased the oxide layers are thin and weak. With this statement, it can be postulated that with high sliding speeds, the oxide layers are removed and remain missing for the most part which allows for severe adhesion wear to take place at a higher rate. The rate of re-growth is influenced by the general passivity of the metal and temperature. The presence of surface contamination is less important when regarding to adhesion of metals at high temperatures (Bowden and Rowe, *The Adhesion of Clean Metals* 1956).

Furthermore, the existence of an oxide film has an effect on the coefficient of friction. It was shown by Hanson et al. that the absence of an oxide layer will cause an increase in the coefficient of friction of the material. The friction force will be relatively low when oxide films are evident on the surfaces but once either film is removed, the coefficient of friction will increase dramatically. The removal of the oxide film happens because of wear. A higher coefficient of friction will result in greater flash temperatures and enable the occurrence of galling even more.

The rise in temperature has a role in the occurrence of galling in this work's case study because there is a strong correlation between temperature and adhesive forces in regards to adhesion wear. At elevated temperatures, there is a softening and growth of the real area of contact which enables higher adhesion and thus wear (Gaard, et al. 2010). The temperature rises due to breakages and energy release from asperities are caused by frictional forces during the rubbing of surfaces. The local surface temperature may rise to a high enough value that enables softening of surface metals at the points of intimate contact between a sliding interaction (Bowden, Moore and Tabor, *The Ploughing and Adhesion of Sliding Metals* 1942). The surface temperature rises exist as short pulses of extreme temperature rises which cause a thermal change in the mechanical properties of a small portion of a surface layer. As the surface temperature gets high, there is an increase in plasticity due to a decrease in strength and a possible phase transformation. If the temperature of a surface layer volume is great enough, welding is realized; this temperature threshold can be referred to as the critical temperature or re-crystallization temperature.

Flash temperature is theorized to be the culprit in this work as the source of temperature. The same surfaces are constantly being rubbed against each other which may lead to even greater temperatures because the flash temperature produces a heat flux. A metaphor for this work's application in regards to the temperature rise is the rubbing of two sticks together to create an ember. The constant rubbing of the sticks, even with a light pressure being applied, will continually raise the localized temperature up to a point. The local area is being given a heat flux for a period of time which would cause an overall temperature increase to the point of flashing. In the case of galling

wear, the temperature is causing the material's yield strength to lower and increase in plasticity. The phase transformation or welding occurrence is critically reliant on the maximum flash temperature rather than the mean temperature (Archard and Rowntree, *The Temperature of Rubbing Bodes: Part 2, The Distribution of Temperatures* 1988).

Though it is difficult to determine which cause precludes the other, the causes of the temperature pulses are from the breakages of asperities and from the work done to cause elastic or plastic flow on the surface. As the surface rub against one another, the extreme temperature pulses will eventually dissipate into the bulk material which will give an overall rise to the metal's body temperature. However, when the rate of dissipation is much smaller than the rate of localized temperature production, one can expect that the micro-volumes of surface layers will exhibit mechanical property changes as a result of critical temperatures being reached.

The thickness of transferred fragment in a galling process is related to the overall heat generation-dissipation balance. Considering a layer of transferred metal, when the adjacent material provides a good heat-sink, energy is easily distributed to a greater volume. The surface layer does not rise an enormous amount and the galled layer is to be expected to be thin in thickness. If the adjacent material is not a good heat-sink, the energy is not able to flow and will be dissipated into the bulk material. In this case the temperature of the galling layer rises significantly and the hardness of the surface is reduced (Markov and Kelly 1999).

It was evident that under certain flow instability inducing conditions, a PRV's disk travels at great speeds and in an oscillatory manner. This leads to galling of surfaces. The speed and oscillations are functions of the force balance of the disk and

the spring-mass system. As the PRV's disk opens, if a flow restriction arises, a flow instability will be incurred since the amount of restriction is a function of the flow. This explains why an oscillation occurs. The magnitude and speed of the oscillation is a function of several items: the spring force, the lifting flow force, static pressures on either side of the PRV's disk, and pressure waves that exist with restrictions on either the inlet or discharge piping. In any case, it was found in this study that under some conditions, galling of the PRV's disk guiding components may not happen if the severity of the disk movement is low. It was also found that if the speed is great enough, galling of components will occur. It was shown by Aldeeb that the speed of a typical PRV's disk during an oscillatory event was 9.1 in/sec [0.23 m/s]. This aligned with Markov and Kelly's criteria listed in Table 1 for the mode of adhesion wear.

Galling is considered to be the form of severe wear since the sliding speed was great enough. Markov and Kelly state that high energy adhesion wear exists when a critical sliding speed is attained; for steels this is 0.4 to 0.7 m/s [1.3 to 2.3 ft/s]. The critical speed between low-energy and high-energy adhesion exist since there is a balance of energy dissipation and friction heat generation. There is a point where the surfaces cannot dissipate the energy at a high enough rate and the surface will change from dislocation plastic flow to an amorphous metal flow. Increasing velocity amplifies the amount of adhered material because high intensity energy is being produced at the surface (Gaard, et al. 2010). The case of galling adhesion wear, Markov and Kelly attest that this happens when the adhesion strength is stronger than one metal surface and equally as strong as or stronger than the other surface. In this scenario, transfer of the soft metal onto the harder one occurs with only partial transfer to the soft metal. In this

works case study where the surfaces had equal hardness which resulted in both surfaces showing wear.

A CFD simulation was used to show that the normal loading of the guiding components within the PRV was low and was found to be approximately 1 lbf [4.45 N]. This force is generated from the surface drag of the disk caused by media flowing against it and towards the outlet side of the PRV. Drag force is a function of the media density, velocity, reference area, and coefficient associated with the component's profile. The value of drag for this case would have been very difficult to accurately determine analytically because the disk's profile cannot be readily approximated and the trajectory of the flow was imperfect; the direction of the flow was not symmetric about the disk. Given this reasoning, it was appropriate to utilize a CFD simulation to determine the drag component. The boundary conditions given to the PRV in the simulation assumed an ideal installation with no flow restrictions or pressure waves occurring. A mass flow based on a theoretical calculation was applied to the outlet; this calculation is presented in the appendix. An inlet static pressure was placed at the inlet of the PRV. These conditions are reflective of a normally operating PRV in an overpressure scenario.

For a gas service application, the flow velocity is expected to be sonic which has been proven in other works. An increase in the set pressure of the PRV would only affect the density of the media flowing about the disk. For the reasoning that the disk's profile and thus drag coefficient and reference area is unchanged with varying set pressures, it is expected that the drag component will be linearly proportional to an increase in set pressure. The CFD simulation showed that the drag for a 100 psig set

pressure was approximately 1 lbf. In the physical testing, a set pressure of 100 and 300 psig was used. It is expected that the 300 psig set pressure would have only a slightly greater value in drag component but is still considered small in terms of galling. Several disk positions were used to determine the maximum drag force on the disk which occurred at 100% open. That is expected since the most amount of flow is able to occur in a fully opened position. The overall results of the simulation confirmed that the normal load applied on the disk and guiding components is low.

The conventional method was used to predict if galling would occur in this situation. The measured movement length in the physical testing and the normal loading was found from the CFD simulation. It was calculated that the amount of volume that should be removed was $2 \times 10^{-11} \text{ in}^3$. This is a very small amount and may be approximated as zero. This result showed that galling wear should not happen in the case given due to the small amount. The normal loading has a large influence on the conventional method's calculation which is why a light load would result in a very small amount of material removal. It is possible that if the surfaces are rubbed a number of times, each time with a very small amount of material transfer, that eventually galling wear would become evident. This could not be determined without the use of equipment with the capabilities of observing this small amount of material. For this study, the value found from the typical method was approximated as being equal to zero.

The friction force was analytically found to be approximately 0.5 lbf [2.22 N] which is expected since the normal loading is small. The actual value for the friction force is questionable because of its dependency to the coefficient of friction. A coefficient value of 0.5 was used in determining the analytical answer. The actual

coefficient it is dependent on many other factors and it is not prudent to assume that the value is constant. As temperature increases, the friction coefficient is likely to change because the surfaces may increase in ductility. Additionally, the value used may not consider the surface finish which has the potential to be dynamic in a wear situation. In any case, the initiating friction force will be low in an application with a small normal load.

The value of the friction force has a large influence of the maximum flash temperature calculation in this work. Utilizing the flash temperature equations and the speeds measured in physical testing, the flash temperature was found to be 220 to 440 F. In other works greater flash temperatures, in excess of 1300 F, were realized. In this work's case study, the lack of normal load likely caused a much lower temperature. The author must express some discretion in the flash temperature calculated in this work. The maximum flash temperature calculated was well below the re-crystallization temperature and not quite great enough to cause a large reduction in strength of the material. During the calculation of the flash temperature, approximations were made for calculating the heat flux generated by frictional heating which most likely lead to possible inaccuracies in the solution. Never-the-less, it is possible that the repeated movement of the components would cause a built-up of temperature great enough to ultimately cause the material to reach a threshold in which its strength is reduced to the point where plastic deformation is enabled and frictional forces cause breakages. The flash temperature equations assume a single rub event, not a repetition of rubbing.

It was found in the physical testing that galling wear was able to take place in a low static load condition and that there is definitely a speed threshold that has to take

place before it can occur. PRV components were subjected to various severities of oscillations. This was done by inducing flow instability in the inlet and outlet portions of the PRV with different levels of restriction. The PRV tested had an API orifice designation of an "E" and had a set pressure of 100 psig for the first and second test run and then 300 psig for the final test run. The first scenario examined was a low severity of flow instability. The PRV exhibited disk position movement which is characterized as flutter. This is simply movement of the disk, but not to a position of totally reclosing and opening. The results of this low severity test run was that the contact points of the disk showed signs of rubbing but not to a galling wear classification extent. The speed observed was 0.3 to 0.36 m/s. The surfaces were observed to be polished and darker than originally. The darkness is from fragmentation of the surfaces but since the speeds were low, there was enough energy present to cause adhesion.

A medium severity test was done with similar results. Though more flow restrictions were applied to the inlet and outlet of the PRV, the disk still exhibited flutter and had similar disk speeds and wear characteristics as the prior test.

In the final case of the flow severity tests, the set pressure was increased to 300psi. This was done by using a spring with a greater stiffness factor. The purpose of this was to increase the force that the set spring would exert on the disk during oscillatory movement. The desired effect of increasing disk movement was achieved by doing this. The final test induced an oscillatory movement that caused the disk to chatter; the position of the disk traveled from open to fully close repeatedly. The distance of movement and speed was greater than the prior two test runs. After this final test run, galling was observed on the disk which is shown in Figure 37. The speed

measured in the final run was 0.45 to 0.9 m/s. Sliding distance of the contact was measured at approximately 0.22 inches.



Figure 37: Galling of Component

The results of galling during the physical testing can be described by Markov's criteria listed in Table 1. It is considered by Markov and Kelly that if the sliding speed is less than 0.4 m/s, the energy rise in an interaction of asperities is not great enough to contribute to catastrophic adhesion wear. In the low and medium flow severity test runs, galling of the surfaces was not observed. The speed of the sliding surfaces was less than 0.4 m/s, which Markov classifies as a low energy type of adhesion wear with subtypes of either seizure or scoring. In the high severity case, the measured speed was greater than 0.4 m/s which is classified as a high energy type of adhesion wear. The theoretical maximum flash temperature calculated, which is equal to the surface temperature, for this application was much less than the crystallization temperature of the metal. From that aspect, this wear was classified as galling. However this does not attest that the temperature did not attribute to the occurrence of the adhesion wear.

Drawbacks to the flash temperature concept is that it is difficult to measure and interpret (Archard and Rowntree, The Temperature of Rubbing Bodes: Part 2, The

Distribution of Temperatures 1988). The flash temperature has a short duration, less than 10^{-3} seconds, and occur on a small location, less than 10^{-4} square meters. Because of the short duration and small affected area, measurements of temperature were not done. Mathematical modeling was not consider due to the realistic variability and complexity of what occurs during a galling event. It would be too simplified for this situation (Karlsson 2012). A transient CFD model was not conducted to simulate disk chatter due to its complexity and relative unimportance towards this work's goal.

This work lends itself to future studies of similar conditions but with an examination of different materials. Other high nickel alloys such as Hastelloy™ would be a worthy investigation. Further research should be done to confirm the existence of galling which would include a detailed metallurgical analysis of the surface structure. A cross section view of a galled layer with hardness probes will help describe the structure of the galled layer. This could then be used to interpret the actual behavior of the wear mechanisms. The leading and trailing edges of the smeared metal layer would help indicate the formation of the layer. Markov and Kelly found that these trailing edges generally have bad contact with the bulk surface. As a result of this, these regions undergo tempering and softening after leaving the friction location source. These high temperatures leave oxide tints which are composed of a martensitic structure; this is a body-centered tetragonal crystal structure. Areas with good adhesion and contact to the bulk surface have an intermixed structure. These areas smear onto the surface and rapidly cool and thus are harder than the two trailing edges. The bulk metal below the surface layer is not hardened. If a sectional analysis of the layer structure were to be done, it would help confirm the thesis of this paper.

It cannot be said with certainty that galling was the only wear mechanism that existed in this application nor can it be stated that it was the initiation stage of the galling process. It can be stated that the final resulting mode of wear was galling. The evidence showed a resemblance of wear that was aligned in orientation to the movement of the sliding surfaces which was characteristic of galling. Furthermore, the conditions measured and calculated agreed with the criterion presented by Markov and Kelly that it can be classified as galling adhesion wear.

Chapter 6: Final Remarks

The main idea of this work provides a theory as to why galling happens in an application of austenitic stainless steel which has a low normal load and a high frequency movement. The initial stage of the sliding movement does not cause severe adhesion wear since the load is small and the surface temperature is not high. As the sliding motion of the surfaces repeat with high speeds, flash temperature occurs and energy is generated as a result. As the temperature increases, the surface aspirates strength lowers and break off from the shear stress. At this point, microscopic amounts of material begin to transfer from the increase in surface energies. The transferred fragments roughen the surfaces and increase the amount of friction and shear forces. Increase in the shear force produces more plastic deformation of the surface layer. As this happens, the fragmentation transfer process perpetuates itself, eventually leading to galling. This phenomenon is exacerbated by the fact that 316 stainless steel has a predisposition to partake in adhesion wear due to its high stacking fault energy and low strength. Additionally stainless steels have a hard surface oxide which has a role in wear. It is suspected that if the oxide is removed from one of the rubbing surfaces, then adhesion would become even more apparent. This is because the stripped surfaces would expose a softer and pure bulk material against a harder oxide layer of the opposing surface. Given all of this, it is attested that this is the reason why galling can exist in a condition of two rubbing surfaces of 316 stainless steel which are lightly loaded and rubbed in an oscillatory manner.

One drawback that was incurred during this work was that the LVDT used was not able to sample the disk positions as quickly as the author would have liked. The

LVDT used was limited in what it could output as far as its position and time-step abilities even when a greater sampling rate was used. A more responsive LVDT and a greater sampling rate would have provided the physical testing done in the work with more accurate velocities. Better position and velocity data would have improved the information collected but the actual data collected was adequate to provide conclusions for this work.

Another aspect the author wishes was available during the data collection was an electron beam microscope. Utilization of this instrument would have provided the ability to observe adhesive material transfer to the surfaces which could have been related with a particular severity of disk movement. This would have also provided the ability to examine surface structures of the transferred metal. The author was reliant on the macroscopic occurrence of adhesion wear to conclude whether galling happened or not. The findings of this work were sufficient to confirm its conjecture but a higher level of detail would have provided additional information. One more instrument that the author wishes was available during this work was a tribometer. This tool would have given accurate control over the normal loading and rubbing speed of the surfaces. This would have enabled a more thorough physical test and generated higher levels of correlated data. The final item that the author wishes was available is the ability to measure flash temperatures. As pointed out by Archard and Rowntree, physical measurements of flash temperatures is highly difficult given the small affected area and short duration the temperatures occur at. This ability would have given this work a high level of detail in terms of showing a relationship between flash temperature and normal loading of a sliding surface.

Surface damage is a complicated topic to model because of the number of potential mechanisms that cause wear and because the wear mechanism changes during the process from work hardening, thermal softening, metal transfer, and the accumulation of wear debris (Markov and Kelly 1999). Furthermore, real world wear situations involve a combination of all classifications of wear (Glaeser 1971). For these reasons, computer modeling of this special case was not done.

In conclusion, the physical testing affirmed the primary postulate of this thesis which was galling can exist when two rubbing surfaces of austenitic stainless steel are subjected to a light normal load and move with great enough speed in an oscillatory manner. It was shown through physical testing that there is a relationship between the speed of the sliding surfaces and the occurrence of galling in a low static load application. Testing showed that when the sliding speed was not great enough, galling did not occur but fragmentation did. When the speed was great enough, galling wear existed. Furthermore, the oscillations were shown to have some role in the happening of galling wear since a single cycle of movement did not indicate galling. It was suspected that the oscillations and flash temperatures had a part in the lowering of the strength of the surface asperities. It was because of the repeated rubbing that the local surface temperature increased. Lastly, austenitic stainless steels have a natural propensity to exhibit galling wear because they have a high stacking fault energy and possess an oxide surface layer. All of the aforementioned statements provided this work with an explanation of the mechanisms involved in the galling of stainless steel surfaces which are subjected to low static contact loads while undergoing a high number of sliding cycles.

References

Aldeeb, A. A., Ron Darby, and Scott Arndt. "The Dynamic Response of Pressure Relief Valves in Vapor or Gas Service. Part II: Experimental Investigation." *Journal of Loss Prevention in the Process Industries Vol 31*, 2014: 127-132.

API. *Standard 520: Sizing, selecting and installation of pressure-relieving devices*. 2013.

Archard, J. F. "The Temperature of Rubbing Surfaces." *Wear Vol. 2*, 1958: 438-455.

Archard, J. F., and R. A. Rowntree. "Metallurgical Phase Transformations in the Rubbing of Steels." *Proceedings of the Royal Society of London. Series A, Mathematical and Physical Sciences, Vol. 418, No. 1855*, 1988: 405-424.

Archard, J. F., and R. A. Rowntree. "The Temperature of Rubbing Bodes: Part 2, The Distribution of Temperatures." *Wear*, 1988: 1-17.

ASTM. "G40-15: Standard Terminology Relating to Wear and Erosioin." West Conshohocken: ASTM International, November 1, 2015.

Bazso, C., and C. J. Hos. "An Experimental Study on the Stability of a Dirct Spring Loaded Poppet Relief Valve." *Journal of Fluids and Structures, Vol. 42*, 2013: 456-465.

Blok, H. "The Flash Temperature Concept." *Wear*, 193: 483-494.

Bowden, F. P., A. Moore, and D. Tabor. "The Ploughing and Adhesion of Sliding Metals." *Journal of Applied Physics*, 1942: 80-90.

Bowden, F. P., and G. W. Rowe. "The Adhesion of Clean Metals." In *Proceedings of the Royal Society of London. Series A, Mathematical and Physical Sciences, Vol. 233, No. 1195*, 429-442. Royal Society, 1956.

Chen, L. H., and D. A. Rigney. "Adhesion Theories of Transfer and Wear During Sliding of Metals." *Wear*, 1990: 223-235.

Cremers, J., L. Friedel, and B. Pallaks. "Validated Sizing Rule Against Chatter of Relief Valves During Gas Service." *Journal of Loss Prevention in the Process Industries*, 2001: 261-267.

Darby, Ron. "The Dynamic Response of Pressure Relief Valves in Vapor or Gas Service, Part I: Mathematical Model." *Journal of Loss Prevention in the Process Industries Vol 26*, 2013: 1262-1268.

Flinn, Richard A, and Paul K Trojan. *Engineering Materials and Their Applications Second Edition*. Boston: Houghton Mifflin Company, 1975.

Gaard, A., N. Hallback, P. Krakhmalev, and J. Bergstrom. "Temperature Effects on Adhesive Wear in Dry Sliding Contacts." *Wear*, 2010: 968-975.

Glaeser, W. A. "Friction and Wear." *IEEE Transactions on Parts, HYbrids, and Packaging, Vol. PHP-7, No. 2.*, June 1971: 99-105.

Hamrock, Bernard J, Steven R Schmid, and Bo Jacobson. *Fundamentals of Machine Elements*. New York: McGraw-Hill, 2005.

Hanson, Magnus, Nils Stavlid, Ernesto Coronel, and Sture Hogmark. "On Adhesion and Metal Transfer in Sliding Contact Between TiN and Austenitic Stainless Steel." *Wear*, 2007: 781-787.

Hellemans, Marc. *The Safety Relief Valve Handbook: Design and Use of Precess Safety Valves to ASME and International Codes and Standards*. Amsterdam: Butterworth-Heinema, 2009.

Hokkirigawa, K., and K. Kato. "An Experimental and Theoretical Investigation of Ploughing, Cutting and Wedge Formation during Abrasive Wear." *Tribology International Vol. 21 No. 1*, 1988: 51-57.

Hsu, K L, T M Ahn, and D A Rigney. "Friction, Wear and Microstructure of Unlubricated Austenitic Stainless Steels." *Wear*, 1980: 13-37.

Jahangiri, M., M. Hashempour, H. Razavizadeh, and H. R. Rezaie. "Application and Conceptual Explanation of an Energy-Based Approach for the Modelling and Prediction of Sliding Wear." *Wear*, 2012: 168-174.

Karlsson, Patrik. "The Early Stage of Galling." Karlstad: Karlstad University, 2012.

LeMay, Iain. *Principles of Mechanical Metallurgy*. New York: Elsevier North Holland, Inc., 1981.

Markov, D., and D. Kelly. "Mechanisms of adhesion-initiated catastrophic wear: Pure Sliding." *Wear*, 1999: 189-210.

Schramm, R. E., and R. P. Reed. "Stacking Fault Energies of Seven Commercial Austenitic Stainless Steels." *Metallurgical Transactions A Volume 6A*, 1975: 1345-1351.

Seah, M. P. "Segregation and the Strength of Grain Boundaries." *Series A, Mathematical and Physical Sciences, Vol 349, No. 1659*. London: The Royal Society Publishing, 1976. 535-554.

Smith, D., J. Burgess, and C. Powers. "Relief Device Inlet Piping: Beyond the 3 Percent Rule." *Hydrocarbon Processing*, 2011: 59-66.

Song, Xueguan, Lei Cui, Maosen Cao, Wenping Cao, Youngchul Park, and William M. Dempster. "A CFD Analysis of the Dynamics of a Direct-Operated Safety Relief Valve Mounted on a Pressure Vessel." *Energy Conversion and Management Vol. 81*, 2014: 407-419.

Appendix A: PRV Specification Sheet and Calculations

Spring Operated Valve Data Sheet

ENG-71000 v.6.8
7-Apr-16
SAK

Page: _____



Customer Name: Paul Hatch
Company:
Location: OU Thesis Research
Phone:
Fax:
Quote #: Induced Chatter Testing
Reference #: Tag Number: Test PRV

PLEASE REFERENCE QUOTE NUMBER ON ALL
CORRESPONDING PURCHASE ORDERS
QUOTE IS GOOD FOR 30 DAYS

Submitted By: _____
Signature: _____
Quote Date: September 21, 2016
Shipping Date: ARO

FLUID DATA	FLUID	FLUID STATE	Air		GAS	
	MOLECULAR WEIGHT	SPECIFIC GRAVITY	29.000		1.000	
	RATIO OF SPECIFIC HEATS	Gas Constant	1.40		356	
	COMPRESSIBILITY FACTOR	REQUIRED CAPACITY	1.000			
SIZING INFORMATION	SUPERIMPOSED CONST BP	SUPERIMPOSED VARI	0.00	psig	0.00	psig
	BUILT-UP BACK PRESSURE	TOTAL BACK PRESSURE	0.00	psig	0.00	psig
	OPERATING TEMPERATURE	RELIEVING TEMPERATURE	60.00	°F	60.0	°F
	OPERATING PRESSURE	ATMOSPHERIC PRESSURE	75.00	psig	14.70	psia
	SET PRESSURE	CDTP	100.00	psig	100.0	psig
	ALLOWABLE OVER PRESSURE		10	psig	/	10.00 %
	INLET PRESS LOSS	FLOWING PRESSURE	0.00	%		124.70 psia
	DISCHARGE COEFFICIENT AND AREAS		ASME, Section VIII, Div. 1			
	VALVE CERTIFICATION / DESIGN CODE		ASME BOILER AND PRESSURE VESSEL CODE, SECTION VIII, DIVISION 1 CERTIFIED			
	SYSTEM TYPE		Vessel or Pipeline			
SIZING RESULTS	REQUIRED AREA	FLOW COEFFICIENT			0.818	
	SELECTED ORIFICE		"E" Orifice		0.212 in ²	
	MAXIMUM CAPACITY OF VALVE AT OVER PRESS.		1818.55 lbs/hr			
	TAG CAPACITY		396.41 SCFM AIR			
	DECIBEL LEVEL	REACTION FORCE	95	dB @ 100 ft	23	lbf <small>WELDED BY PRESSURE OVER PRESSURE</small>
MATERIALS	VALVE BODY MATERIAL	INLET MATERIAL	WCB CARBON STEEL		CARBON STEEL	
	BONNET MATERIAL	BONNET TYPE	CARBON STEEL		CLOSED	
	NOZZLE MTRL	NOZZLE TYPE	316 STNLS STL		SEMI NOZZLE	
	DISK MATERIAL		316 STNLS STL			
	SEAT MATERIAL	O-RING MATERIAL	15% GLASS PTFE		STD (FLUOROCARBON & BUNA-N)	
SPRING MATERIAL		17-7 PH STAINLESS STEEL				
OPTIONS	1/4" PIPE TAP		YES			
	SOUR GAS SERVICE		NO			
	CAP TYPE		CLOSED CAP			
VALVE INFORMATION	VALVE TYPE		9100 THREADED			
	PART NUMBER		91-17E51T09X1T			
	INLET X OUTLET		1" MNPT x 1" FNPT			
	CENTER TO FACE DIMENSIONS		A = 3-1/4 in.		B = 1-7/8 in.	
REPAIR KIT NUMBER		1E1T1X1				
PRICING INFORMATION	QUANTITY	PRICE PER VALVE	1			
	TOTAL PRICE	(US \$)				
ALL PRICES ARE NET PRICES IN US DOLLARS						
DISCLAIMER	<p>As per ASME code, Section VIII, Division 1, para. UG-125(a), the customer accepts all responsibility in insuring that the correct pressure relief valve is installed for their application. The purchase order for the pressure relief valve confirms the sizing calculations and material compatibility choices made by Mercer Valve are correct for the application. This sizing program does not take material compatibility or pressure and temperature limitations into account for choosing materials. Please verify all material choices with Mercer Valve Company, Inc.</p> <p>Other company names and product names used in this document are the registered trademarks or trademarks of their respective owners.</p>					
NOTES	When backpressure is greater than 10psi, chatter should occur.					

Figure 38: PRV's Specification Sheet

Customer Name: Paul Hatch
Company:
Location: OU Thesis Research
Phone:
Fax:
Quote #:
Reference #: Induced Chatter Testing
Tag Number: Test PRV



Equation Used to Size Safety Relief Valve

P_1	$=$	P_{set}	$+$	$P_{overpressure}$	$-$	$P_{inletloss}$	$+$	P_{atm}
124.7	=	100.0	+	10.0	-	0	+	14.7

$$A = \frac{V}{6.32 \times C \times K_d \times P_1 \times K_c} \sqrt{\frac{T \times Z \times M}{1}}$$

$$A = \frac{V}{6.32 \times 356 \times 0.818 \times 124.7 \times 1 \times 0.212} \sqrt{\frac{1}{520 \times 1 \times 29}}$$

$A = \text{in}^2 < 0.212 \text{ in}^2$ "E" Orifice

Equations are taken from API STD 520 Part 1 9th Edition
 P_1 = Flowing Pressure, psia
 P_{set} = Set Pressure, psig
 $P_{overpressure}$ = Allowable Overpressure typically 3psi or 10% of Set pressure, psig
 $P_{inletloss}$ = inlet piping losses, psig
 P_{atm} = Atmospheric Pressure, psia
 V = Required Flow Rate, scfm
 C = Gas Constant as a function of cp/cv
 K_d = Discharge Coefficient
 K_c = Combination Correction Factor
 T = Relieving Temperature at Nozzle, Rankine
 Z = Compressibility Factor
 M = Molecular Weight
 A = Required Area, in²
 A_0 = Orifice Area, in²

Note:
1) ALL UNITS ARE CONVERTED TO PSI, SCFM, IN², AND RANKINE.

Figure 39: PRV's Sizing Calculations Sheet

Appendix B: Additional CFD Study Results

Table 5: 100% Lift Raw Data

Goal Name	Unit	Value	Averaged Value	Minimum Value	Maximum Value	Progress [%]	Use In Convergence	Delta	Criteria
Lift Force Up on Disk	[lbf]	41.667	41.4609	41.0092	41.6667	100	Yes	0.658	1.0751
Force Side on Disk	[lbf]	1.0046	1.0095	0.996	1.0219	100	Yes	0.02	0.0576

Table 6: 75% Lift Raw Data

Goal Name	Unit	Value	Averaged Value	Minimum Value	Maximum Value	Progress [%]	Use In Convergence	Delta	Criteria
Lift Force Up on Disk	[lbf]	38.904	38.7496	38.3475	38.904	100	Yes	0.556	1.1024
Force Side on Disk	[lbf]	1.0596	1.0548	1.0478	1.061	100	Yes	0.013	0.0762

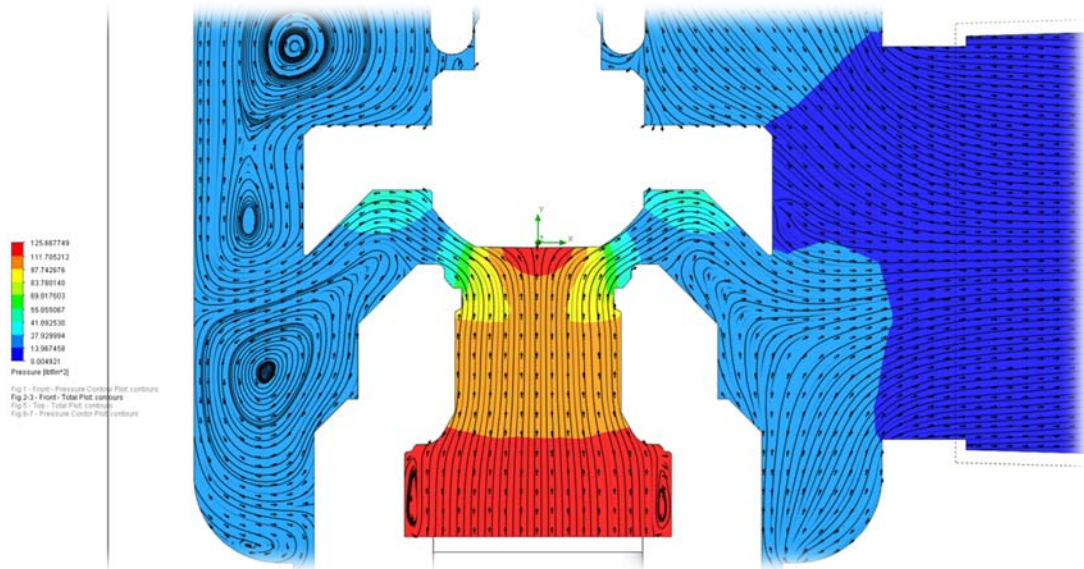


Figure 40: 75% Lift Pressure and Flow Profiles

Table 7: 50% Lift Raw Data

Goal Name	Unit	Value	Averaged Value	Minimum Value	Maximum Value	Progress [%]	Use In Convergence	Delta	Criteria
Lift Force Up on Disk	[lbf]	32.367	32.2337	31.8609	32.3668	100	Yes	0.506	0.9114
Force Side on Disk	[lbf]	0.9356	0.9269	0.9124	0.9356	100	Yes	0.023	0.0719

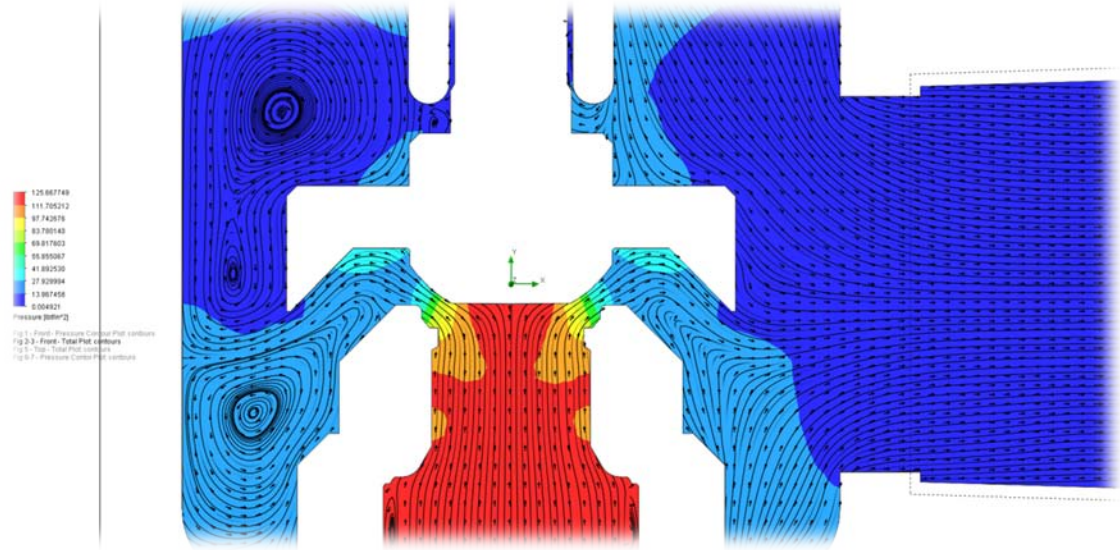


Figure 41: 50% Lift Pressure and Flow Profiles

Table 8: 25% Lift Raw Data

Goal Name	Unit	Value	Average Value	Minimum Value	Maximum Value	Progress [%]	Use In Convergence	Delta	Criteria
Lift Force Up on Disk	[lbf]	21.663	21.5199	21.038	21.6644	100	Yes	0.626	0.6456
Force Side on Disk	[lbf]	0.6414	0.6095	0.5815	0.6414	100	Yes	0.025	0.0458

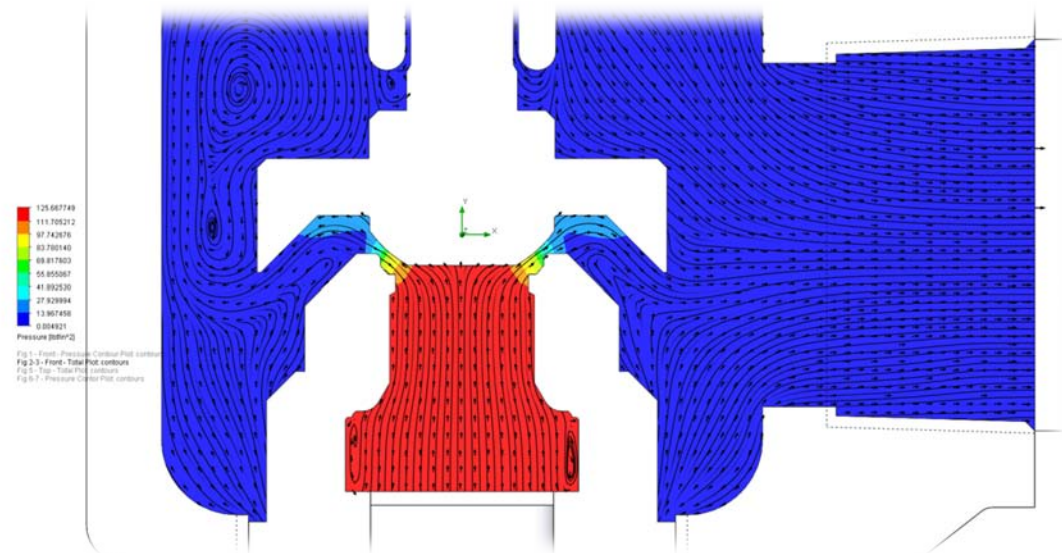


Figure 42: 25% Lift Pressure and Flow Profiles

Table 9: 5% Lift Raw Data

Goal Name	Unit	Value	Averaged Value	Minimum Value	Maximum Value	Progress [%]	Use In Convergence	Delta	Criteria
Lift Force Up on Disk	[lbf]	14.087	14.1124	14.0872	14.1292	100	Yes	0.042	0.481
Force Side on Disk	[lbf]	0.3042	0.2946	0.2856	0.3042	100	Yes	0.007	0.0072

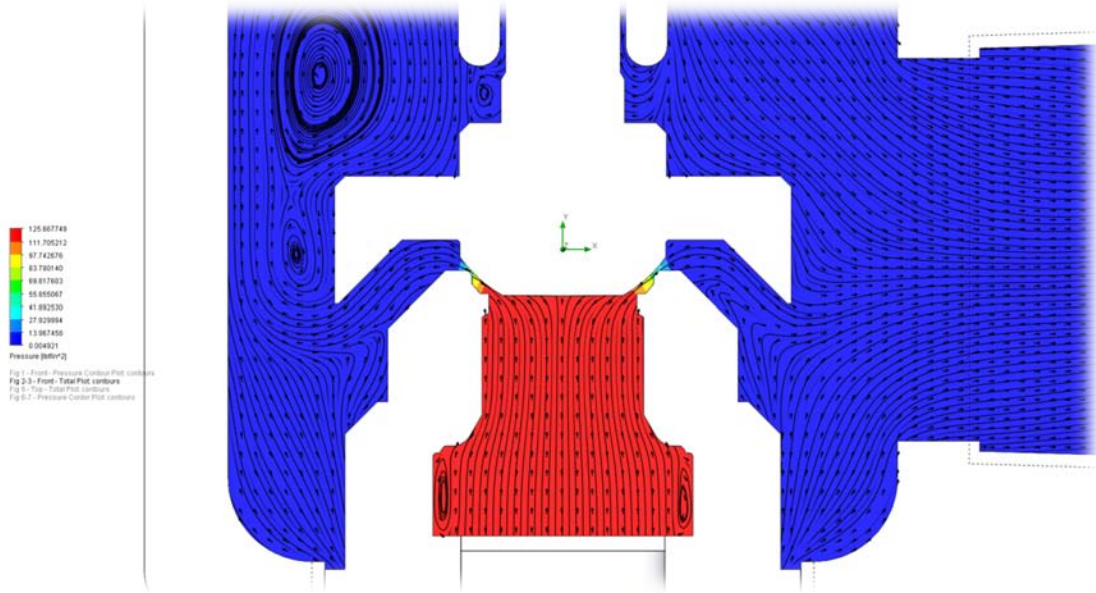



Figure 43: 5% Lift Pressure and Flow Profiles

Appendix C: Component Material Certification



81-102002
DISK STEM
9-3-2014
PO 71629
PG 1 OF 2

Page 01 of 02
Certification Date
23-JUL-2014

CUSTOMER ORDER NUMBER
072214SL4

CUSTOMER PART NUMBER
525402

EARLE M. JORGENSEN COMPANY
1800 N UNIVERSAL AVENUE
KANSAS CITY MO 64120

Invoice Number
S140562

SOLD TO: MIDWEST SCREW PRODUCTS, INC. **SHIP TO:** MIDWEST SCREW PRODUCTS, INC

13426 B STREET 13426 B STREET
OMAHA NE 68144 OMAHA NE 68144

Description: 316/316L CF ANN BAR
3/8 RD X 12' R/L DFARS COMPLIANT **Line Total:** 139 LB
HEAT: L4R8 **ITEM:** 525402

Specifications:

AMS 5648 L	AMS 5653 G	ASTM A276 10
ASTM A479 13A	ASME SA479 10A	QQ S 763 B
UNS 31600/31603	EN 10204 3.1	ASTM A484 13A
ASTM A182 13	ASME SA182 10	ASTM F899 11
QQ S 763 F	ASTM A320 CL1 B8M 08	ASTM A193 10A
ASME SA193 CL1 B8M 10	ASTM A262 PR E	DFARS 252.225-7008
ASTM A751 08		

CHEMICAL ANALYSIS

C ✓ 0.026	CO ✓ 0.32	CR ✓ 16.52	CU ✓ 0.27	MN ✓ 1.26	MO ✓ 2.00	N ✓ 0.041	NI ✓ 10.50
P ✓ 0.037	S ✓ 0.0265	SI ✓ 0.28					

RCPT: R307091 **COUNTRY OF ORIGIN :** USA
VENDOR: NORTH AMERICAN STAINLESS

MECHANICAL PROPERTIES

DESCRIPTION	YLD STR KSI	ULT TEN KSI	%ELONG IN 02 IN	%RED IN AREA	HARDNESS BHN
	86.58 ✓	102.99 ✓	34.15 ✓	75.46 ✓	213

GRAIN SIZE : 4 - 6

1780
81-102002

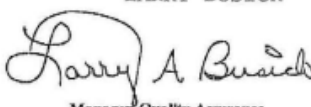
The above data were transcribed from the manufacturer's Certificate of Test after verification for completeness and specification requirements of the information on the certificate. All test results remain on file subject to examination.

We hereby certify that the material covered by this report will meet the applicable requirements described herein, including any specification forming a part of the description.

The willful recording of false, fictitious, or fraudulent statements in connection with test results may be punishable as a felony under federal statutes.

Material did not come in contact with mercury while in our possession.

LARRY BUSICK



Manager, Quality Assurance

Figure 44: Material Composition of Disk Stem

KB/917



METALLURGICAL TEST REPORT

6870 Highway 42 East
Ghent, KY 41045-9615
(502) 347-6000

Certificate: 945404 17 Mail To: COPPER AND BRASS SALES, INC. SOUTHFIELD MI 48066-
Ship To: COPPER AND BRASS SALES, INC. 8001 HURDLY WAY NORWOOD OH 43619
Date: 5/03/2014 Page: 1 of 1
Steel: 316/316L
Finish: Cold Draw
Dia/Thk: .6250 in
Leg Length: Length: 144.00 in
Corrosion: ASTM A262 Prac E OK
Customer: 0925 045
NAS Order: LP 17489 4
Your Order: 5400218266 Item Code: SSRD00046

PRODUCT DESCRIPTION:
Round Bar, Annealed, Cold Draw
UNS 31600/31603 EN 10204 3.1, ASTM A484/13a
ASTM A276/13, ASTM A479/13a, ASTM A182/13 CHEM ONLY,
ASME SA479/13, ASME SA182/10 CHEM ONLY, ASTM F899/11
AMS 5648L/AMS 5653H, AMS QQS-763B, QQS 763P
SOLUTION ANNEAL TEMP 1900F MIN, ASTM A320/08 CL 1 GR B8M
ASTM A193/10A-ASME SA193/10 CL 1 GR B8M

REMARKS:
COMPLIES W/REQUIREMENTS OF DEPAR 252.225-7009 EU DIRECTIVE
2011/65/EU-ROHS. EAF+AOD+CC. NO WELD REPAIR. MELTED AND MFG
IN USA FREE FROM MERCURY AND LOW MELTING ALLOY CONTAMINATION

91-022002
ADJ SCREW
1/9/2015
PO 72963
1 OF 1

Bundle Weight	Bundle Weight	Bundle Weight	Bundle Weight	Bundle Weight	Bundle Weight	Bundle Weight	Bundle Weight	Bundle Weight	Bundle Weight
R023032	2202								

CHEMICAL ANALYSIS CM(Country of Melt) ES(Spain) US(United States) ZA(South Africa) JP(Japan) Chemical Analysis per ASTM A751/08

Heat	Supplier #	CM	C %	CO %	CR %	CU %	MN %	MO %	N %	NI %	P %	S %
L779		US	.027	.31	16.60	.31	1.44	2.07	.052	10.52	.030	.0295
			SI %									
			.33									

MECHANICAL PROPERTIES

Id	EB	No.	.2YS KSI	UTS KSI	RA %	Elong % 4D
R023032	R L	217.0	82.24	101.36	65.61	63.01

MERCER VALVE CO., INC.
CERTIFIED TRUE COPY

NAS hereby certifies that the analysis on this certification is correct. Based upon the results and the accuracy of the test methods used, the material meets the specifications stated. These results relate only to the items tested and this report cannot be reproduced, except in its entirety, without the written approval of NAS

Technical Dept. Mgr. ERIC HESS

John G. Jambelli

Del.: 2403385469
CSP# 34780
DATE: 09/12/2014

FROM: ThyssenKrupp Materials NA
Cust. RW SCREW PRODUCTS INC
Cstar
Wgt.: 450 LB

PO# 34780

Figure 45: Material Composition of Adjustment Screw